

Challenges in conditioning a stochastic geological model of a heterogeneous glacial aquifer to a comprehensive soft dataset.

Julian Koch<sup>1,2,\*</sup>, Xin He<sup>2</sup>, Karsten Høgh Jensen<sup>1</sup>, Jens Christian Refsgaard<sup>2</sup>

<sup>1</sup>Department of Geosciences and Natural Resource Management, University of Copenhagen

<sup>2</sup>Department of Hydrology, Geological Survey of Denmark and Greenland

Submitted to:

HESS – Hydrology and Earth System Sciences

\*Corresponding Author Address:

Julian Koch

Department of Hydrology

Geological Survey of Denmark and Greenland (GEUS)

Øster Voldgade 10

Copenhagen, Denmark

E-mail: juko@geus.dk

Telephone: +45 38142768

16     Abstract

17     In traditional hydrogeological investigations, one geological model is often used based on subjective  
18     interpretations and sparse data availability. This deterministic approach usually does not account for any  
19     uncertainties. Stochastic simulation methods address this problem and can capture the geological structure  
20     uncertainty. In this study the geostatistical software TProGS is utilized to simulate an ensemble of  
21     realizations for a binary (sand/clay) hydrofacies model in the Norsminde catchment, Denmark. TProGS  
22     can incorporate soft data, which represent the associated level of uncertainty. High density (20m x 20m x  
23     2m) airborne geophysical data (SkyTEM) and categorized borehole data are utilized to define the model  
24     of spatial variability in horizontal and vertical direction, respectively and both are used for soft  
25     conditioning the TProGS simulations. The category probabilities for the SkyTEM dataset are derived  
26     from a histogram probability matching method, where resistivity is paired with the corresponding  
27     lithology from the categorized borehole data. This study integrates two distinct datasources into the  
28     stochastic modeling process that represent two extremes of the conditioning density spectrum; sparse  
29     borehole data and abundant SkyTEM data. In the latter the data has a strong spatial correlation caused by  
30     its high data density, which triggers the problem of overconditioning. This problem is addressed by a work  
31     around utilizing a sampling/decimation of the dataset, with the aim to reduce the spatial correlation of the  
32     conditioning dataset. In the case of abundant conditioning data it is shown that TProGS is capable of  
33     reproducing non-stationary trends. The stochastic realizations are validated by five performance criteria:  
34     (1) Sand proportion, (2) mean length, (3) geobody connectivity, (4) facies probability distribution and (5)  
35     facies probability – resistivity bias. As conclusion, a stochastically generated set of realizations soft  
36     conditioned to 200m moving sampling of geophysical data performs most satisfying when balancing the  
37     five performance criteria. The ensemble can be used in subsequent hydrogeological flow modeling to  
38     address the predictive uncertainty originated from the geological structure uncertainty.

39     Key words: Geological model, stochastic simulation, geophysical data, soft conditioning, model  
40     performance, TProGS

## 1. Introduction

Constraints in accurate and realistic solute transport modeling in hydrogeology are caused by the difficulty of characterizing the geological structure. The subsurface heterogeneity heavily influences the distribution of contaminants in the groundwater system. The scale of heterogeneity is often smaller than the data availability (e.g. borehole spacing). In traditional hydrogeological studies, one geological model is built based on the best comprehensive knowledge from often sparse borehole data and subjective interpretations. This can lead to alleged correct results, for instance when addressing the water balance on catchment scale, but will often prove to be inadequate for simulations beyond general flows and heads, e.g. contaminant transport modeling. Therefore, it is proposed by numerous studies that the uncertainty on the geological conceptualization is crucial when assessing uncertainties on flow paths (Neuman, 2003; Bredehoeft, 2005; Hojberg and Refsgaard, 2005; Trolborg et al., 2007; Seifert et al., 2008). One of the strategies often recommended for characterizing geological uncertainty and assessing its impact on hydrological predictive uncertainty is the use of multiple geological models (Renard, 2007; Refsgaard et al., 2012).

In this respect geostatistical tools such as two-point statistics e.g. TProGS (Carle and Fogg, 1996; Carle et al., 1998) and multipoint statistics (MPS) (Caers and Zhang, 2002; Strebelle, 2002; Caers, 2003; Journel, 2004) are powerful tools as they enable the generation of multiple equally plausible realizations of geological facies structure. This study targets the realistic description of heterogeneity in a geological model by introducing diverse data into the stochastic modeling process to generate a set of equally plausible realizations of the subsurface using geostatistics (Refsgaard et al., 2006).

61 In geostatistical applications field observations can constrain the simulation as soft or hard conditioning.  
62 “Hard conditioning” forces the realizations to honor data completely whereas “soft conditioning” honors  
63 the data partly with respect to the uncertainty of the observation (Falivene et al., 2007). This feature is  
64 essential because it enables the user to associate uncertainties to the conditioning dataset that can be of  
65 either subjective or objective nature. Incorporating a comprehensive and continuous soft conditioning  
66 datasets to a stochastic simulation such as TProGS is challenging. Alabert (1987) published an early study  
67 on the implications of using sparse soft conditioning data to a stochastic simulation. The analysis shows  
68 that soft conditioning significantly increases the quality of the realizations. The same was also observed  
69 by McKenna and Poeter (1995) where soft data from geophysical measurements could significantly  
70 improve the geostatistical simulation. In the past years, highly sophisticated geophysical methods and  
71 advanced computational power allow stochastic simulations that are conditioned to a vast auxiliary  
72 dataset. This poses new challenges to the data handling and to the simulation techniques.

73 Chugunova and Hu (2008) present a study where continuous auxiliary data is introduced directly, without  
74 classification to a MPS simulation data in addition to the general training image. MPS requires a site  
75 specific training image that represents the geological structure accordingly, which is often the main  
76 source of uncertainty in MPS simulations. The above mentioned MPS studies conduct mostly 2D  
77 simulations, partly on synthetic data. The training image is the backbone of the MPS method and it has  
78 been acknowledged by dell'Arciprete et al. (2012) and He et al. (2013) that reliable 3D training images  
79 are difficult to acquire.

80 Alternative methods to integrate vast auxiliary information (e.g. geophysics) into the modeling process  
81 and at the same time force local accuracy are collocated cokriging or cosimulation techniques (Babak and

82 Deutsch, 2009). Here a linear relationship between the auxiliary variable and the target variable is built in  
83 a model of cross covariance. The essentially linear relationship is often too restrictive and does not  
84 represent the complex physical processes. Mariethoz et al. (2009b) present a prospective method that  
85 extends the collocated simulation method by using a model of spatial variability of the target variable and  
86 a joint probability density distribution to depict the conditional distribution of the target variable and the  
87 auxiliary variable at any location.

88 The method of anchored distributions (MAD) (Rubin et al., 2010) is a suitable approach for the inverse  
89 modeling of spatial random fields with conditioning to local auxiliary information. Structural parameters  
90 such as global trends and geostatistical attributes are considered in a conditional simulation. The  
91 conditioning is undertaken by anchored distributions which statistically represent the relationship between  
92 any data and the target variable.

93 The truncated plurigaussian simulation method (Mariethoz et al., 2009a) generates a Gaussian field for  
94 the target and the auxiliary variable using variogram statistics. These Gaussian fields are truncated to  
95 produce categorical variables that represent the hydrofacies. The truncation is controlled by threshold  
96 values that can be defined in a “lithotype rule” that represents the general geological concept. It is a very  
97 flexible method, because conceptual understandings are easily incorporated, but non-stationarity and  
98 especially directional depended lithotype rules are difficult to incorporate.

99 TProGS is a well-established stochastic modeling tool for 3D applications and it has been successfully  
100 applied to simulate highly heterogeneous subsurface systems by constraining the simulation to borehole  
101 data (Carle et al., 1998; Fleckenstein et al., 2006). Weissmann et al. (1999), Weissmann and Fogg (1999)

102 and Ye and Khaleel (2008) use additional spatial information obtained from soil surveys, sequence  
103 stratigraphy and soil moisture, respectively for accessing the complex lateral sedimentary variability and  
104 thus improving the quality of the model in terms of spatial variability. It has not been tested whether  
105 TProGS, is capable of handling abundant soft conditioning data. Moreover, the risk that a cell-by-cell soft  
106 constraining may cause an overconditioning of the simulation has not been fully investigated.  
107 Overconditioning is defined by the authors as an effect triggered by dense and spatial correlated  
108 conditioning data that produces an altered picture of observable uncertainties. Therefore the self-  
109 consistency of the stochastic simulation is questioned, because soft constraining should be treated  
110 accordingly during the simulation.

111 Recent studies by Lee et al. (2007) and dell'Arciprete et al. (2012) highlight that TProGS is comparable  
112 with other geostatistical methods like, multi-point statistics, sequential Gaussian simulations and  
113 variogram statistics (Gringarten and Deutsch, 2001). The distinct strength of TProGS is the simple and  
114 direct incorporation of explicit facies manifestations like mean length, proportion and (asymmetric)  
115 juxtapositional tendencies of the facies.

116 Geophysical datasets are valuable information in many hydrogeological investigations. It can  
117 considerably improve the conceptual understanding of a facies or hydraulic conductivity distribution and  
118 identify non-stationary trends. However, the integration of geophysical data and lithological borehole  
119 descriptions is often difficult. A recent study by Emery and Parra (2013) presents an approach to combine  
120 borehole data and seismic measurements in a geostatistical simulation to generate multiple realizations of  
121 porosity. Hubbard and Rubin (2000) review three methods that allow hydrogeological parameter  
122 estimation based on geophysical data. The three methods link seismic, ground penetrating radar (GPR)

123 and tomographic data with sparse borehole data to support the hydrogeological description of the study  
124 site. Our study integrates high resolution airborne geophysical data with borehole data to build a  
125 probabilistic classification of the subsurface at site. The geophysical data are collected by SkyTEM, an  
126 airborne transient electromagnetic method (TEM) that has been used extensively in Denmark for the  
127 purpose of groundwater mapping (Christiansen and Christensen, 2003; Jorgensen et al., 2003b; Sorensen  
128 and Auken, 2004; Auken et al., 2009). This study utilizes a method that translates SkyTEM observation  
129 data into facies probability which enables associating the geophysical data with softness, according to the  
130 level of uncertainty. Very few studies have integrated high resolution airborne geophysical data in a  
131 stochastic modeling process (Gunnink and Siemon, 2009; He et al., 2013).

132 Most stochastic studies only make relatively simple validations of how well the simulations are able to  
133 reproduce known geostatistical properties. Carle (1997) and Carle et al. (1998) investigate the goodness  
134 of fit between the simulated and the defined model of spatial variability. The geobody connectivity is  
135 used by dell'Arciprete et al. (2012) to compare results originated from two- and multipoint geostatistics.  
136 Chugunova and Hu (2008) make a simple visual comparison between the auxiliary variable fracture  
137 density and stochastic realizations of the simulated fracture media. A more advanced validation is  
138 conducted by Mariethoz et al. (2009b) where simulated variograms and histograms are compared with  
139 reference data for the simulation of synthetic examples. In spite of these few studies that have addressed  
140 the validation issue, no guidance on which performance criteria to use and how to conduct a systematical  
141 validation of a stochastic simulation has been reported so far.

142 It should be noted that we in line with Refsgaard and Henriksen (2004) do not use the term model  
143 validation in a universal manner, but in a site specific context where a model validation is limited to the

144 variables for which it has been tested as well as to the level of accuracy obtained during the validation  
145 tests.

146 The objectives of this study are: (1) to set up TProGS for a study site based on lithological borehole data  
147 and high resolution airborne geophysical data and investigate the effect of the two distinct conditioning  
148 datasets to the simulation; (2) to assess the problem of overconditioning in a stochastic simulation; (3) to  
149 ensure that non-stationary trends are simulated accordingly by TProGS; and (4) to identify and test a set  
150 of performance criteria for stochastic simulations that allow the validation against geostatistical properties  
151 derived from field data. The results of the present study are intended for application in a hydrological  
152 modeling context (Refsgaard et al., 2014).



## 153 2. Study Site

154 Figure 1 shows the 101 km<sup>2</sup> Norsminde catchment, located on the east coast of Jutland south of Aarhus.  
155 The topography allows a separation between an elevated western part, with changing terrain and a  
156 maximum elevation of 100 m and a flat and low elevated eastern part, where the coastline represents the  
157 eastern boundary. Glacial morphologies, namely moraine landscapes are predominant in most of the  
158 catchment. The geological stratigraphy indicated by borehole logs encompasses Paleogene and Neogene  
159 marine sediments underlying a heterogeneous stratigraphy of Pleistocene glacial deposits. The Paleogene  
160 sediments are characterized by very fine-grained impermeable marl and clay. Above the Neogene  
161 sequence shows sandy formations encased by a clay-dominated environment with Miocene marine  
162 sediments. The entire Miocene sequence varies in thickness up to 40 m and the sandy formations reach  
163 thicknesses of more than 10 m. The Miocene sequence is only present in the western part of the  
164 catchment where the stochastic modeling is conducted and forms the lower boundary of the simulation  
165 domain. Thus, only the upper Pleistocene glacial sequence is modeled. The glacial deposits in the western  
166 part of the catchment contain both sandy and clayey sediments, where clay is predominant. Borehole logs  
167 indicate that the Pleistocene clay spans from glaciolacustrine clay to clay till. Within the clay  
168 environment, the sandy units are allocated in small units and vary between gravel, meltwater-sand and  
169 sandy tills. The total thickness of glacial sediments varies between 10 and 40 m with heterogeneous  
170 distributions of the mostly glaciofluvial sand features between less than a meter and 20 m in thickness.  
171 The subject to the stochastic modeling, the delineated Pleistocene glacial sequence in the western part,  
172 provides interesting challenges like distinct heterogeneity and a diverse terrain.

### 173 3. Data

174 Two different sources of data, namely lithological borehole data and airborne based geophysical data  
175 (SkyTEM) are used, where the former is utilized to describe the vertical sand and clay variability and the  
176 latter for assessing the lateral direction.

#### 177 3.1. Borehole Data

178 The borehole dataset contains 112 borehole logs with varying depths. The descriptions in the borehole  
179 reports are converted to a categorical binary (sand/clay) system at 5 cm vertical discretization. Further  
180 each borehole's uncertainty is validated according to the method of He et al. (2014). The uncertainty  
181 assessment allows defining individual trust scores and thus the definition of how much each borehole  
182 should constrain the conditional simulation in the form of soft data. Drilling method, age, purpose of  
183 drilling, among others are used as variables to ensure a systematic approach to validate the uncertainty of  
184 each individual borehole. The boreholes are grouped into four quality groups with 100%, 95%, 90% and  
185 85% as trust scores. The classified borehole dataset states an overall sand proportion of 30%.

#### 186 3.2. Geophysical Data

187 The geophysical dataset comprises resistivity data from SkyTEM helicopter surveys. The SkyTEM  
188 method has been extensively used for subsurface mapping in Denmark (Jorgensen et al., 2003a;  
189 Jorgensen et al., 2005), where it has proven to be a successful tool for hydrogeological investigations.  
190 SkyTEM data have the advantage of a high spatial resolution in the top 20 to 30m and at large spatial  
191 coverage. However, some studies rise concern about the accuracy of interpretations of deep soundings  
192 (Andersen et al., 2013). In the Norsminde catchment data were collected at 2000 flight km containing  
193 over 100,000 sounding points. The distance between the flight lines is between 50 and 100 m. The  
194 dataset is processed with a spatially constrained inversion algorithm (Schamper and Auken, 2012)  
195 giving a 3D distribution of the underground resistivity. The sounding data were interpolated to a 20m x  
196 20m x 2m grid domain by using 3D kriging as the interpolation method. The gridded resistivity data can  
197 be utilized as a proxy for lithology, as high and low resistivity cells indicate a high probability of sand

and clay, respectively. Bowling et al. (2007) conduct a detailed study on the relationship between sediment and resistivity at a field site. Resistivity is linked to grainsize distribution and is used to delineate mayor geological structures. A strong positive correlation between gravel content in the lithology and resistivity is observed.

The SkyTEM dataset covers approximately 85% of the delineated glacial sequence. Figure 2 shows the spatial variation of the median resistivity for a 4- and a 16- subarea grid. Higher median resistivity values are located in the southern part of the glacial sequence. This indicates a greater sand proportion in the given areas. The conclusion of the spatial pattern in Figure 2 is that stationarity cannot be attested to the glacial sequence. This will have implications for the stochastic simulation.

The exact sand proportion can be derived by introducing a cut off value that divides the SkyTEM dataset into a sand and a clay fraction. Jorgensen et al. (2003b) estimate resistivity thresholds to differentiate between sediments in buried valleys in Denmark. Accordingly, glacial sand has a resistivity greater than 60  $\Omega\text{m}$  whereas clayey till sediments are placed between 25 and 50  $\Omega\text{m}$  and thus the exact cut off value varies between study sites.

### 3.3. Data integration

Figure 3 underlines some of the associated problems of the data integration of geophysical SkyTEM data and borehole descriptions. The lithological information from the borehole interprets thin layers of meltwater sand confined by clay in the top few meters. The SkyTEM data with a vertical resolution of two meters cannot capture this small scale variability. This supports to use geophysical data only for the lateral model of spatial variability and to incorporate the fine descriptions from the borehole data for the vertical model of spatial variability.

He et al. (2014) developed a method to manually calibrate the cut off value by comparing borehole with SkyTEM data at different spatial domains with the aim to reduce the deviation in sand proportion between the two data types. It is assumed that the deviation has to be minimized at domains with a high borehole density where the boreholes are assumed to best represent the domain conditions. It is shown

223 that a borehole density of 2 per km<sup>2</sup> reduces the representative error and that 46 Ωm as cut off value  
224 reduces the deviation in sand proportion between the two datasets. The calibrated cut off value yields a  
225 sand proportion of 23%.

226 Further He et al. (2014) developed a histogram probability matching (HPM) method that enables a direct  
227 translation from resistivity into facies probability. Resistivity is paired with the lithological borehole  
228 description at the coinciding cell. The data pairs are grouped in 10 Ωm bins and for each bin the sand/clay  
229 fraction is first calculated and then plotted as a histogram. 3<sup>rd</sup> order polynomial curve fitting is applied to  
230 the histogram and the manually calibrated cut off value is superimposed to the fitted curve (Figure 4). The  
231 shape of the curve reflects the lumped uncertainties from both datasets. The flatness of the transition  
232 zone, around 50%, sand probability indicates a high uncertainty for the corresponding resistivity values.  
233 There are many sources of uncertainty that will affect the relationship between electrical conductivity and  
234 facies information. The HPM-method lumps various sources and the shape of the fitted curve reflects  
235 those, especially the width of the transition zone. He et al. (2014) discussed the prevalent uncertainties:  
236 first, borehole descriptions are not accurate, and classification of borehole lithology is subjective. Second,  
237 there are uncertainties on the resistivity data due to the resolution of the physics itself, the geophysics  
238 instruments, field measurements and signal processing (inversion). Third, there is no unique relationship  
239 between resistivity and lithology, and the curve can therefore be fitted in various ways. Last, there are  
240 uncertainties related to the scale of aggregation, since the borehole data and geophysical data have  
241 different resolutions and hence different supporting scales. The HPM-method used in this study is study  
242 site specific and is purely based on spatial correlations and is not build up on physical relationships.  
243 Therefore it cannot be transferred to other catchments, however the relationship between resistivity and  
244 facies is manually calibrated for this site and is thus expected to be valid.

245 The HPM-method is a probabilistic approach and it is preferred to deterministic model  
246 approaches, because of its suitability for soft conditioning in a stochastic geological simulation.  
247 In a more deterministic sense, a positive correlation between resistivity soundings and hydraulic

248 conductivity estimates derived from pumping test has been acknowledged for glacial outwash  
249 aquifers (Urish, 1981). Linde et al. (2006) review different strategies to relate geophysical and  
250 hydrogeological properties and attest that geophysics undoubtedly add value to a  
251 hydrogeological characterization. One suggested approach, which would be suitable for  
252 SkyTEM data for the estimation of hydrogeophysical parameters, is the joint inversion, where  
253 the geophysical or the hydrogeological inversion utilizes hydrogeological or geophysical data,  
254 respectively. Another review paper by Slater (2007) address joint inversion methods as well as  
255 petrophysical relations between geophysical (electrical) properties and effective hydraulic  
256 properties (pore volume and pore surface) at core and field scale, which allow direct mapping of  
257 hydraulic properties (Kemna et al., 2004). Slug tests with an estimate of the local saturated  
258 hydraulic conductivity are available for the Norsminde catchment. However, due to differences  
259 in scale, a low number of slug tests and unclarity of the correlation we found the direct mapping  
260 approach unfeasible for our study.

## 261 4. Methods

### 262 4.1. TProGS – Transition Probability Geostatistical Software

263 The geostatistical software TProGS is applied in this study. It is based on the transition probability (TP)  
264 approach (Carle and Fogg, 1996; Carle et al., 1998). Continuous Markov Chain models (MCM) are used  
265 to represent the model of spatial variability (Krumbein and Dacey, 1969; Carle and Fogg, 1997; Ritzi,  
266 2000). TProGS allows for the simulation of multiple realizations by utilizing a sequential indicator  
267 simulation (SIS) (Seifert and Jensen, 1999) and by performing simulated quenching (Deutsch and  
268 Cockerham, 1994; Carle, 1997). These two steps are mutually dependent and they make sure that the  
269 realizations honor local conditioning data as well as the defined model of spatial variability.

270 The major advantage of TProGS is that fundamental observable attributes are parameterized in the  
271 modelling process: volumetric fractions (proportions), mean lengths (thickness and lateral extent) and  
272 (asymmetric) juxtapositional tendencies. These attributes can be assessed by data analysis and geological  
273 interpretations and control the shape of the MCM model. The facies proportion is related to the  
274 asymptotic limit of the MCM. The mean length is indicated on a plot of auto-transition probabilities as  
275 the intersection of the tangent at the origin with the x-axis. Asymmetric juxtapositional tendencies are of  
276 interest when simulating a system with at least three categories and can thus be neglected in this study.  
277 TProGS computes the realizations of the geology in two uncoupled, but mutually dependent steps. An  
278 initial configuration of facies distribution is produced by the SIS algorithm (Deutsch and Journel, 1992).  
279 Secondly, the initial configuration is reshuffled by the simulation quenching optimization algorithm  
280 (Deutsch and Cockerham, 1994). The TProGS simulation domain of this study is discretized into 20m x  
281 20m x 2m cells on a 450 x 600 x 40 cell grid. The horizontal transition probabilities (TP) are based on  
282 SkyTEM data, that is categorized by a cut off value of 46  $\Omega$ m and the vertical extent is purely based on  
283 borehole data.

## 284 4.2. Split Sample Test

285 The two incorporated conditioning datasets are very distinct and will affect the simulation in opposite  
286 ways: sparse borehole data allow large simulation freedom whereas dense SkyTEM data limit the  
287 simulation freedom. Naturally they will be combined in order to condition the simulation to the best  
288 combined knowledge of the system. However it is of interest to know how each individual conditioning  
289 dataset affects the simulation. In this context a split sample test can reveal valuable information: one  
290 simulation conditioning to purely borehole data and the other one conditioned to purely SkyTEM data. It  
291 will be tested how well the simulations conditioned to borehole data reproduce the high resistivity cells,  
292 where a high sand probability is evident and how well the simulations conditioned to SkyTEM data  
293 reproduce the locations with borehole information.

## 294 4.3. Moving Sampling

295 Most studies on stochastic modeling condition the simulation to sparse data. In this study a  
296 comprehensive cell-by-cell soft conditioning dataset is applied and it is anticipated that this may result in  
297 overconditioning. Decimating the conditioning dataset out is a very intuitive sampling approach to work  
298 around the problem of overconditioning. However, if the resampled conditioning dataset is too sparse,  
299 information from the original dataset might not be sufficiently accounted for. Thus the tradeoff between  
300 two extremes, too much and too few data is investigated. Opposed to the static sampling technique a  
301 moving sampling method is applied.  $n$  different location grids with the same distance between the  
302 samples for each chosen distance (100m, 200m, etc.), where each has an accumulated shift of the origin  
303 (+ sampling distance/ $n$  in X and Y direction). For the 100m moving sampling approach the first sampling  
304 grid has the origin (0,0) the second (20,20), the third (40,40), etc. For the TProGS application in this  
305 study five location grids are generated, which yields five independent soft conditioning datasets. Five  
306 realizations are computed for each soft dataset; giving a total of 25 realizations. In addition to the  
307 comparison between moving and static sampling, different sample densities are also be tested.

## 308 4.4. Sampling scenarios

309 In total, eight conditioning scenarios are tested in this study. For the split sample test two scenarios are  
310 used, namely purely borehole data (*'onlyBH'*) and purely cell-by-cell SkyTEM data (*'onlySky20'*). In the  
311 following both datasources are combined to represent the best combined knowledge of the system.  
312 Further, static and moving sampling are applied: Borehole data and SkyTEM data sampled statically at  
313 20m, 100m, 200m and 500m (*'BH-Sky20static'*, *'BH-Sky100static'*, *'BH-Sky200static'* and *'BH-*  
314 *Sky500static'*, respectively). Moving sampling is tested at 100m and 200m sampling distance (*'BH-*  
315 *Sky100moving'* and *'BH-Sky200moving'*, respectively).

#### 316 4.5. Performance criteria

317 Five performance criteria are defined to evaluate an ensemble of realizations of the geology. They aim for  
318 validating the ensemble with respect to the TProGS input, namely the defined model of spatial variability  
319 (mean length and proportion) and the soft conditioning dataset. The five performance criteria test the self-  
320 consistency of TProGS and thus if all input parameters and data are treated accordingly. The glacial  
321 structure in the Norsminde catchment represents only approximately 20% of the entire TProGS  
322 simulation domain and deviations in simulated spatial statistics between the entire model domain and the  
323 simulation target are expected.

##### 324 4.5.1. Sand proportion

325 The deviation between the mean simulated sand proportion and the defined sand proportion in the MCM  
326 can be calculated for a set of realizations. The focus should be on the target area only, the area that will be  
327 extracted from the rectangular model domain for subsequent applications. The analysis of the sand  
328 proportion is based on 25 realizations.

##### 329 4.5.2. Mean length

330 The simulated mean length can be estimated by recalculating the TPs from the TProGS output for the  
331 target area only. The simulated TPs for a set of realizations can be averaged (10 realizations in this case)



332 and compared with the measured TPs to estimate the deviation in mean length between the predefined  
333 and the mean simulated length.

#### 334 4.5.3. Geobody connectivity

335 The degree of connectivity of permeable areas in the subsurface has major implications for flowlines and  
336 particle ages. Renard and Allard (2013) conducted a methodology study on various static and dynamic  
337 connectivity metrics. These metrics can be utilized as a comparison and interpretation indicator for  
338 multiple stochastically generated realizations of the geology. The work by dell'Arciprete et al. (2012)  
339 shows the successfully implementation of connectivity metrics to compare stochastic realizations  
340 computed by two- and multi-point statistics. Giudici et al. (2011) underline that evidence of a single  
341 “best” connectivity metric is still missing and further research is necessary in that field.

342 For this study two static connectivity metrics,  $\theta$  and  $\Gamma$ , are selected. They refer to the first and second  
343 geobody connectivity defined by Hovadik and Larue (2007). A geobody is defined as one connected 3D  
344 cluster of sand. Hence it is a distinct sand feature that is confined by clay. The architectural elements are  
345 interpreted on a 20m x 20m x 2m scale.

$$346 \quad \theta = \frac{V_l}{\sum_{i=0}^n V_i} \quad \text{Eq.1}$$

$$347 \quad \Gamma = \frac{\sum_{i=0}^n (V_i)^2}{(\sum_{i=0}^n V_i)^2} \quad \text{Eq.2}$$

348 where  $V_i$  is the volume of an individual geobody,  $n$  is the number of unconnected geobodies and  $V_l$  is the  
349 volume of the largest occurring geobody.  $\theta$  represents the ratio of the volume of the largest geobody to  
350 the total volume. Denoted as  $\Gamma$  is the proportion of the pairs of cells that are connected among the entire  
351 pairs. The two selected connectivity metrics originate from the percolation theory, which describes the  
352 transition from many disconnected clusters to one large coherent cluster. This is mainly depending on the  
353 facies proportion. As the proportion gradually increases it reaches a point where one big cluster appears.

354 The percolation threshold is expected to be approximately 0.59 and 0.31 for a 2D and 3D grid,  
355 respectively (Hovadik and Larue, 2007). Mean values of  $\theta$  and  $\Gamma$  are computed based on 10 realizations.

#### 356 4.5.4. Facies probability distribution

357 The facies probability distribution reflects the inter variability among a set of realizations and can be  
358 extracted from a probability map. Each cell in the probability map reflects the simulated category  
359 probability within a set of realizations. The comparison between the distribution of the original soft  
360 dataset, which constrains the simulation and the simulated facies probability distribution, allows  
361 validating the performance of the simulation. Ideally the distribution of the original soft dataset is  
362 reproduced by the simulation, which does not allow assumptions concerning the accuracy of the  
363 allocation pattern of the simulated facies probability.

#### 364 4.5.5. Facies probability – resistivity bias

365 The validation of the facies probability – resistivity bias depicts if the simulated facies probability  
366 corresponds to the fitted curve derived from the histogram probability matching method, and thereby test  
367 whether the simulated facies probability is according to the resistivity pattern. The simulated facies  
368 probability value is paired with the coinciding resistivity value of the gridded SkyTEM dataset. The pairs  
369 are grouped in 5  $\Omega\text{m}$  bins and the median values of simulated facies probability can be plotted for each  
370 bin. Further the RMSE can be calculated between the simulated facies probability and the fitted curve at  
371 each bin in order to quantify the agreement.

## 372 5. Results

### 373 5.1. TProGS setup

374 The computed transition probabilities (TP) and the fitted Markov Chain model (MCM) for both  
375 horizontal and vertical direction are given in Figure 5. A sand proportion of 23% and a mean length of a  
376 sand lens of 5m and 500m for vertical and horizontal direction respectively yield MCMs that are in good

377 agreement with the measured TPs. Figure 3 indicates an increasing gradient in sand proportion from north  
378 to south. This non-stationary trend is also shown in Figure 5 where the additional sand-sand transition  
379 MCMs are plotted that fit measured TP data from the northern and southern subdomain; defined by 13%,  
380 2m, 400m and 30%, 5m and 600m respectively. 25 realizations are generated based on the MCMs that are  
381 specified in Figure 5.

## 382 5.2. Split sample test

383 Two sets of 25 realizations are computed. The entire conditioning dataset is split into two parts, in order  
384 to analyze the effect of both extremes of the conditioning spectrum: Abundant data (*onlySky20*) and  
385 sparse data (*onlyBH*).

### 386 5.2.1. Visual comparison

387 Figure 6 presents two individual realizations (a) and (b) and the resulting probability maps (c) and (e)  
388 from both conditioning datasets at an elevation of 49m. Examining the individual realizations reveals that  
389 the spatial variability is much greater for the *onlyBH* scenario results. This is reasonable, because the  
390 amount of constraining data is also much less. This conclusion is supported by the probability maps. The  
391 probability map computed from the *onlySky20* conditioning scenario shows only little inter variability  
392 among the 25 realizations and resembles almost a binary sand and clay image. The *onlyBH* scenario  
393 simulates a probability map that shows high inter variability among the computed realizations, but the  
394 high probable sand areas do not coincide with the high resistivity areas in the SkyTEM data (d), because  
395 many large sand features are not captured by borehole data. On the other hand, some high probable sand  
396 features in the *onlyBH* scenario are not represented by the *onlySky20* scenario, because small sand  
397 features that are indicated by the borehole data are not detected by the SkyTEM survey.

### 398 5.2.2. Quantitative comparison

399 High resistivity areas are defined by a minimum resistivity value of 60  $\Omega\text{m}$  which is equivalent to 70%  
400 probability of sand occurrence based on the fitted histogram curve in Figure 4. The results of the split

sample test are given in Table 1. The *onlyBH* scenario allocates only 20.1% of the high resistivity cells accordingly. Also, only 74.3% of the cells, where the lithology in the borehole reports shows sand are simulated correspondingly. Some of the borehole data are treated as soft data, which enables the simulation to overwrite the lithological information, during the SIS and the simulated quenching. This will happen especially when sand lenses are very thin and vertically confined by clay. The *onlySky20* scenario simulates 44% of those cells accordingly and allocates almost all high resistivity cells as sand. However, almost 60% of the high resistivity cells are simulated with 100% sand probability. This is in poor agreement with field data, because the fitted histogram curve does not exceed sand probability values higher than 85% (Figure 4). The SkyTEM dataset indicates a large high resistivity cluster in the south-west at an elevation of 49 m (Figure 6), which is not detected at all by the borehole dataset, because there is only one borehole penetrating this area.

#### 5.2.3. Local comparison

Figure 7 shows the vertical profile of one borehole (99.918) that penetrates the sand cluster and compares the simulation results from the *onlyBH* and *onlySky20* scenarios. The borehole has a trust score of 95%. While both datasets agree on the top layer being sandy and the occurrence of a thick clay layer below 75 m followed by a sand layer, they disagree on the location of the deeper sand layer. In the borehole data this sand deeper sand layer is detected at an elevation of 45m and below, whereas the SkyTEM dataset indicates sand occurrence approximately 8m higher; 53m and below. This discrepancy between 45m and 53 m has considerable implications for the simulation results at 49 m shown in Figure 6. However, one borehole alone will not be sufficient to substantially influence the simulation over large areas. Marginal amplification of the *onlyBH* scenario is noticeable at borehole 99.918. On the other hand, sand probabilities are clearly amplified in the *onlySky20* scenario; everything above 0.5 is amplified close to 1.0 and everything below 0.5 close to 0. The results from Table 1 and Figures 6 and 7 support the assumption of overconditioning caused by the comprehensive cell by cell soft conditioning.

#### 5.3. Overconditioning

426 The observed problem of overconditioning is caused by spatially correlated data which are incorporated  
427 into the modeling process. A very intuitive approach to work around the problem of overconditioning is  
428 decimating the SkyTEM dataset by only sampling part of it. This will only be necessary in horizontal  
429 direction because the correlation length of the data is much less in the vertical direction. There is a  
430 tradeoff between the correctly simulated facies probability and the accuracy of the spatial allocation  
431 pattern. To illustrate this tradeoff three resampled conditioning scenarios are compiled: 100m, 200m and  
432 500m sampling distance in X- and Y-direction and at the same time also including the boreholes for  
433 conditioning. For each of the three conditioning scenarios (*BH-Sky100static*, *BH-Sky200static* and *BH-*  
434 *Sky500static*, respectively) 25 realizations are computed and the probability maps for sand are presented  
435 in Figure 8. The simulated probability maps of the *BH-Sky100static* and *BH-Sky200static* conditioning  
436 scenarios are visually almost identical. Therefore only the latter is shown (d) and the image reflects  
437 already a higher variability than the results by the *BH-Sky20static* scenario (c). Reducing the conditioning  
438 data density increases the uncertainty of sand or clay. But at the same time the accuracy of correctly  
439 locating sand or clay units decreases, because the *BH-Sky500static* scenario (e) shows high probable sand  
440 areas which are not indicated by the original dataset (b). If for instance a high resistivity cell embedded in  
441 low resistivity cells is sampled for the conditioning, this cell may generate a sand lens in the out thinned  
442 conditioning scenario but would be limited by the neighboring cells in the *BH-Sky20static* scenario. The  
443 moving sampling method can improve the spatial coverage of the conditioning datasets and thus improve  
444 the quality of a set of realizations.

445 Again, the high resistivity cells are investigated to analyze if the bigger sand lenses are simulated  
446 correctly by the different conditioning datasets (Table 2). It is evident that the percentage of cells at the  
447 extreme ends of the simulated sand probability falls drastically after decimating the soft data out. The  
448 100m distance scenarios still allocates more than 80% of the high resistivity correctly. On the other hand,  
449 the *BH-Sky500static* performs poorly, by only simulating 32.7% of the high resistivity cells correctly. It is  
450 also evident that the differences between static and moving sampling are small with regard to the correct  
451 allocation of the higher resistivity cells.

#### 5.4. Performance criteria

For further validation of the different sampling distances (20m, 100m, 200m and 500m) and sampling schemes (static and moving) the five identified performance criteria will be applied to quantify the quality of the simulations.

##### 5.4.1. Sand proportion

Table 3 shows the defined sand proportions of the delineated glacial structure. In order to investigate non-stationarities the model domain is additionally subdivided into north and south. The SkyTEM dataset indicates a higher sand fraction in the southern part compared to the north, 30% and 13% respectively. The simulated sand proportions for the *BH-Sky20static* scenario show a good agreement with the defined values. Larger deviations are evident for the *BH-Sky200moving* scenario. Both conditioning scenarios are capable of reproducing the non-stationarity of the system, in regard to the sand proportion. The sand proportions are somewhat overestimated for *BH-Sky200moving* scenario, and much less for the *BH-Sky20static* scenario. Also the overestimation of simulated sand proportion in the northern subarea is larger than in the southern subarea.

##### 5.4.2. Mean length

The comparison of the early (first lag = 100m) measured and simulated TPs for the sand-sand transitions in X- and Y-direction allows to validate how well the lateral mean length is simulated by TProGS. Figure 9 comprises the measured TPs in horizontal direction, the fitted MCM and the computed mean TPs for the *BH-Sky20static* scenario and *BH-Sky200moving* scenario, based on 10 realizations, for the total and the sub-domains. The effect of overconditioning is very evident, as the computed mean TPs based on 20m sampling conditioning data purely represent the original measured TP values. Since no simulation freedom is present, the MCM cannot control the output. On the contrary, the *BH-Sky200moving* scenario computes mean TPs that are more independent from the original data and rather follow the defined MCM. The mean length of a sand lens can be derived by the steepness of the tangent where the lag approaches zero. In general, the TP at lag 0 and 100 m are simulated too low; indicating that the simulated mean size

477 of a sand lens is too small. This is more prominent in results by the *BH-Sky200moving* scenario. It is  
478 evident that the non-stationarity of the mean length of a sand lens is represented accordingly, although it  
479 is undersimulated at all domains.

#### 480 5.4.3. Geobody connectivity

481 For the categorized SkyTEM data  $\theta$  and  $\Gamma$  are computed as 98.7% and 99.3%, respectively. This shows  
482 values close to unity and should not be seen as a real reference, rather as a benchmark, because the  
483 extreme low variability picture does not account for any uncertainties. The TProGS simulations based on  
484 the two conditioning scenarios both undersimulate the connectivity metrics. The *BH-Sky20static* scenario  
485 yields negative deviations of 2.1% and 1.1%, respectively and the *BH-Sky200moving* scenario 2.8% and  
486 1.4%, respectively. The results indicate that  $\theta$  and  $\Gamma$  show a similar behavior, where  $\Gamma$  appears to be  
487 decreasingly greater as the proportion increases. Values close to unity and the very small deviations are in  
488 good agreement with the general percolation theory, which sets the percolation threshold to  
489 approximately 30% for 3D grids (Hovadik and Larue, 2007).

#### 490 5.4.4. Facies probability distribution

491 Figure 10 shows the probability distribution for all discussed conditioning scenarios, with static (a) and  
492 moving (b) sampling, with 25 realizations in each set. The original soft data distribution has its maximum  
493 at approximately 20% and less than 5% are with either 0% or 100% sand probability. The *BH-Sky20static*  
494 scenario simulates approximately 70% of the cells with zero change and thus has an extremely poor fit  
495 with the soft dataset and the overconditioning is very prominent. It appears that overconditioning  
496 amplifies the conditioning values to the extremes (e.g. 0.6 is simulated as 1.0 and 0.4 as 0.0, Figure 7).  
497 The *BH-Sky500static* scenario reproduces the probabilities from the original soft dataset well, with only  
498 approximately 10% zero change cells. However, the allocation pattern shows small resemblance with the  
499 original dataset (Figure 8, (b)). *BH-Sky100static* scenario gives an intermediate solution, as the  
500 probability is better reproduced than with the *BH-Sky20static* scenario, but still, more than 20% of the  
501 cells are simulated as purely either sand or clay within the ensemble. Nevertheless, the *BH-Sky100static*

502 scenario is dense enough to capture the full variability of the system, as indicated by the original SkyTEM  
503 dataset. Additionally the results of the *BH-Sky200static* scenario are plotted in (a). The number of zero  
504 variability cells is decreased to approximately 20% and the maximum at 20% sand probability is close to  
505 the original soft dataset. Figure 10, (b) compares the static with the moving sampling approach for the  
506 100m and 200m distance scenarios. The simulated facies probability distribution shows no differences for  
507 the static and moving 100m distance scenarios. However, at 200m sampling distance, the two sampling  
508 techniques are distinguishable, as the moving sampling yields fewer zero variability cells than the static  
509 sampling.

#### 510 5.4.5. Facies probability – resistivity bias

511 The results are given in Figure 11 for the static sampling (a) and the moving sampling approach (b). The  
512 strong amplification of the resulting probabilities originating from the *BH-Sky20static* scenario is obvious  
513 in (a). The *BH-Sky500static* scenario performs poorly, especially in high resistivity areas, because those  
514 areas are not sufficiently covered by the 500m sampling distance. A better fit is represented by the *BH-*  
515 *Sky100static* scenario, because the amplification is much lower than for the *BH-Sky20static* scenario,  
516 especially for high resistivity areas. On the other hand, low resistivity areas are more amplified than high  
517 resistivity areas. The *BH-Sky200static* scenario gives a satisfying fit with the original fitted curve,  
518 especially in high resistivity areas, which indicates that the high probable sand cells are mostly allocated  
519 correctly by the model. The simulated facies uncertainty for the low resistivity cells is rather amplified  
520 by the *BH-Sky200static* scenario. Figure 11, (b) investigates the simulation differences caused by the  
521 static and moving sampling approach. The behaviour is similar to Figure 10, (b), because the differences  
522 for the 100m distance scenarios are marginal, while the *BH-Sky200moving* scenario generates a slightly  
523 lower facies probability – resistivity bias than the *BH-Sky200static* scenario. The RMSEs between the  
524 fitted curve (Figure 4) and the simulations show that the *BH-Sky200moving* and *BH-Sky200static*  
525 sampling conditioning scenarios perform best, both with a RMSE of 0.06. Comparable are the *BH-*  
526 *Sky100moving* and *BH-Sky100static* sampling conditioning scenarios with a RMSE of 0.09 and 0.08,  
527 respectively. The *BH-Sky20static* scenario performs poorest with a RMSE of 0.2.



## 528 6. Discussion

### 529 6.1. Choice of geostatistical method

530 The choice of the stochastic method for this study is application driven (Refsgaard et al., 2014). In the  
531 Norsminde catchment, it is evident from both borehole and geophysical data that the glacial sequence  
532 contains till clay and sand lenses distributed in extremely irregular patterns that are non-stationary.  
533 Without dense conditioning data the heterogeneous and non-stationary structures will not be simulated  
534 correctly. TProGS allows conditioning and operates a straight forward way to build the model of spatial  
535 variability. In multi-point statistics (MPS) the definition of a reliable 3D training image is challenging,  
536 especially when simulating extremely irregular patterns (Honarkhah and Caers, 2012). Defining a MPS  
537 training image for the Norsminde catchment is peculiar, because it could only be based on interpreted  
538 SkyTEM data; with inflated length scales in the vertical direction. This makes the model of spatial  
539 variability in TProGS more reliable and objective, because it is based on measured transition probabilities  
540 and not on an interpreted training image. Further the transition probabilities are based on the data type we  
541 trust best: borehole data in the vertical- and SkyTEM data in the horizontal direction.

542 However, MPS is broadly applied in 2D and 3D applications: The snesim algorithm (Liu, 2006)  
543 combines object-based and pixel-based methods in the general MPS framework, to enforce spatial pattern  
544 reproduction and local conditioning, respectively. It was successfully applied by He et al. (2013) in a 3D  
545 application. Another promising approach is given by Chugunova and Hu (2008), where MPS is tested on  
546 non-stationary 2D structures, by continuous soft conditioning to a secondary variable. Here two training  
547 images from the geological structure and from the secondary variable are joint in the simulation.

548 Many promising geostatistical methods have advanced to incorporate auxiliary information to constrain  
549 the simulated target variable: Truncated plurigaussian simulation (Mariethoz et al., 2009a), collocated  
550 simulation with probability aggregation (Mariethoz et al., 2009b). Most of them are only tested on 2D  
551 applications partly with synthetic data. This present study uses TProGS as the geostatistical tool, because

552 of its reliable model of spatial variability and further it is well established in 3D applications with sparse  
553 conditioning data.

## 554 6.2. TProGS setup

555 Direct transformation of geophysical data, such as SkyTEM, into a deterministic subsurface model is  
556 risky, because too much reliance on geophysical mapping can lead to seriously wrong hydrogeological  
557 models (Andersen et al., 2013). Uncertainties are expected in both, geophysical and lithological data and  
558 the shape of the fitted histogram curve reflects those. High uncertainty is associated with the transition  
559 zone; around 50% sand probability. Although the cut off value that divides the SkyTEM dataset into sand  
560 and clay is calibrated, there is a large quantity of high uncertain cells included which make the measured  
561 TPs directly dependent on the cut off value. Therefore the facies proportion and mean length are very  
562 sensitive to the selection of the cut-off value. As a result, the MCM in the lateral direction, as part of the  
563 TProGS setup, is highly dependent on the way the SkyTEM data is treated. Difficulties in the integration  
564 of the two data types are indicated in Figure 2. Small scale heterogeneities indicated by the borehole  
565 descriptions are not represented by the coarser SkyTEM dataset. This supports computing the horizontal  
566 and vertical TPs individually using SkyTEM and borehole data, respectively.

567 The SkyTEM dataset used in the present study is a 3D grid of 20m x 20m x 2m which was spatially  
568 interpolated from soundings with distances of about 17 m and 50-100 m along and between the flight  
569 lines, respectively. To reduce the overconditioning problem it might have been preferable to use the direct  
570 sounding data instead of the interpolated dataset. A similar effect is achieved by resampling, but here  
571 interpolated data with a higher uncertainty than the direct soundings are used.

572 Simulating a binary system is a crude simplification of the broad range of sediments in the glacial  
573 sequence. However, classifying the SkyTEM data into discrete facies or deriving the soft information on  
574 facies membership are peculiar in a multi facies environment. Additionally less abundant facies (e.g.  
575 gravel) will show extremely uncertain correlations in the histogram probability matching method. Last the  
576 less abundant facies might be represented on a 20m domain, but it will often not be visible on the 100m

577 domain chosen for the subsequent hydrological flow simulations. Dell'Arciprete et al. (2012) present a  
578 study where geostatistics are implemented to simulate small scale heterogeneities in a multi facies  
579 environment.

### 580 6.3. Data footprint

581 Borehole and SkyTEM data are integrated by the histogram probability matching method (He et al., 2014)  
582 where differences in support scale are partly neglected. The support scales of the two data types are  
583 expected to vary. The lithological data from the boreholes are aggregated to 2m to be in better vertical  
584 agreement with the geophysical dataset. The agreement in the lateral direction is more questionable,  
585 because the footprint increases with depth for the geophysical data. The footprint is approximately 15-  
586 20m on the surface and in the range of 50m at 30m penetration depth. Further the footprint will depend on  
587 the material; with a larger energized volume for high conductance materials (high clay content). The two  
588 steps of processing the sounding data, namely inversion and kriging are both expected to inflate the  
589 footprint by smoothing values. However one can assume that the chosen grid size of 20m x 20m x 2m is  
590 suitable for near surface resistivity values, because the footprint of the geophysical data is constantly  
591 smaller than the correlation length, which is approximately 500m in vertical direction and 5m in lateral  
592 direction.

### 593 6.4. Split sample test

594 Both datasources have advantages and disadvantages: Borehole data have a higher data certainty and a  
595 finer spatial resolution in the vertical extent to better represent smaller sand features, but are essentially  
596 undersampled in the lateral extend. On the other hand, SkyTEM data have a good spatial coverage and  
597 represent the bigger sand features well, but at the same time the data are associated with a higher data  
598 uncertainty. At this point, four major sources of uncertainty can be defined: (1) The inversion that  
599 transforms the SkyTEM measurement into resistivity, (2) the borehole data, (3) the relationship between  
600 lithology and resistivity and (4) the footprint mismatch between small scale borehole data and large scale  
601 SkyTEM data. So it is precarious to assume the SkyTEM data as true geology, but it can serve as a

reference/benchmark when validating the simulation results. The *onlyBH* scenario does not capture all of the main sand features, which are revealed by the SkyTEM survey: Only 20% of the high resistivity cells, where the resistivity is greater than  $70\Omega\text{m}$  are simulated correctly. For the *onlySky20* scenario only 44% of the sand descriptions in the boreholes are simulated correctly, which underlines that the SkyTEM data does not measure the finer sand features correctly. The conducted split sample test does not allow to draw firm conclusions on simulation performance, it rather analyses the agreement between the two dataset propagated through the model.

## 6.5. Overconditioning

Correlated data, both temporally and spatially are a common problem in hydrogeological investigations. It has not been previously reported how TProGS is able to handle such a conditioning dataset. TProGS stochastically simulates the subsurface facies system by utilizing the two mutually dependent steps SIS and simulated quenching. Soft information is not considered accordingly during the cokriging of the local probability estimate in the SIS step nor is it completely accounted for in the objective function used for the simulated quenching in the latest TProGS version. However Deutsch and Wen (2000) successfully integrate exhaustive soft data in simulated quenching, which shows that the algorithms are generally capable of incorporating soft data.

Work around methods have to be developed to overcome the problems associated with overconditioning. Decimating the soft conditioning dataset may seem as an overly simplistic and very crude approach, but the study aims at finding the balance between too few data and too many data. The risk to miss important features is high when conditioning to too few data. This study mainly deals with the latter case, where too many data lead to an underestimation of the simulation uncertainty. Including a moving sampling strategy ensures that the spatial variation in the original dataset is best represented. A drawback of this approach is that valuable information might be lost, which again underlines the need for model validation, where the entire geophysical dataset is used for the evaluation. The decimation approach works as a very pragmatic solution for a study-specific problem and

its generalization might be limited. Decimating the SkyTEM dataset out and only considering data on a 200m spaced moving sampling grid gives the most satisfying results. A 200m sampling distance is expected to be sufficient to adequately capture all relevant geological features proxied by the entire dataset; this can be argued by the fraction between the observed mean length and the conditioning spacing. The mean length of a sand lens is found to be 500m and can proxy the correlation length. With a horizontal length scale of 500m and sampling at 200m we still condition the simulation with two to three soft data points in each horizontal direction for each mean sized sand feature.

Concluding it cannot be directly concluded that overconditioning is a general problem in stochastic simulations where a vast conditioning dataset is applied. However it can be presume that heavily spatially correlated data will affect also other stochastic simulation algorithms. TProGS was clearly not developed to run with such comprehensive conditioning. To our knowledge, the problem of overconditioning has not yet been reported nor discussed and with our study we would like to create awareness. In regard to the technique of geophysical prospecting it can be concluded that the problem of overconditioning is clearly not limited to airborne based TEM data.

## 6.6. Performance criteria

We identified and tested five performance criteria for validating the model.

(1) *Sand proportion*. Artificial conditioning data outside the target area honoring the defined proportion and MCM may help to make the simulation more homogeneous. In that context, exhaustive hard conditioning outside the simulation target can be tested.

(2) *Mean length*. The simulated and measured TPs are compared by Carle (1997) and Carle et al. (1998). (Carle et al., 1998) simulate a four category system and the simulated quenching yields a perfect match between the modeled TPs and the defined MCM. On the other hand, Carle (1997)

underlines that small deviations are to be expected and shows this by various examples where different SIS and simulated quenching parameters are tested.

(3) *Geobody connectivity*. The connectivity is partly dependent on the proportion. The sand connectivity for the simulation based on the *BH-Sky200moving* scenario is simulated lower and the sand proportion higher in comparison to the results from the *BH-Sky20static* scenario. This shows that the geobody connectivity is not fully depending on the proportion in this study. However it is a more feasible performance criterion for proportions far below the percolation threshold.

(4) *Facies probability distribution*. A good agreement between the simulated facies probability distribution and the original soft dataset doesn't ensure that the allocation pattern of the simulated probability is correct. This becomes evident when validating the results of the *BH-Sky500static* scenario.

(5) *Facies probability – resistivity bias*. The simulated facies probability should be in agreement with a corresponding resistivity observation to ensure that the spatial allocation pattern is simulated correctly. All bins are weighted the same, neglecting the inequality of data in each bin.

We used 25, 10 and 10 realizations to compute the first three performance criteria, respectively. Computing a moving average shows that the mean converges to +/-2% deviation to the final mean after ca. 15 realizations for the first criterion and after ca. 5 realizations for the second and third criteria, which justifies the selected number of realizations. The two latter criteria incorporate the computed probability map based on 25 realizations. Probability maps proved to be a useful tool to investigate the inter variability among realizations (Alabert, 1987; Carle, 2003; Mariethoz et al., 2009b). The results of the *onlyBH* scenario show the highest inter variability and a moving average tested at 10 random locations in the grid shows that after 20 realizations the mean converges to less than +/-20% from the final mean and to less than +/-10% after 23 realizations. These numbers are supposed to decrease as the conditioning data increase and therefore are 25 realizations in the analysis of the two latter criteria justifiable.

Table 4 compiles the five performance criteria for two different TProGS simulations: The *BH-Sky20static*- and the *BH-Sky200moving* scenario. A weighted and balanced analysis of the performance

676 criteria helps to identify the best result. For example, if only considering sand proportion and mean  
677 length, it can be argued that the validation favors the *BH-Sky20static* scenario. However both, the facies  
678 probability distribution as well as the facies probability - resistivity bias attest poor performance. On the  
679 other hand, if interpreting the probability distribution only, it seems that the validation favors the *BH-*  
680 *Sky500static* scenario. Collectively, the conclusion is that the *BH-Sky200moving* scenario generates the  
681 overall most balanced results.

## 682 7. Acknowledgments

683 This work has been a part of the NiCA (Nitrate Reduction in a Geologically Heterogeneous Catchment)  
684 project ([www.nitrat.dk](http://www.nitrat.dk)), which is funded by the Danish Council for Strategic Research.

685

686 8. References

- 687 Alabert, F., Stochastic imaging of spatial distributions using hard and soft information, M. S. thesis,  
688 1987.
- 689 Andersen, T. R., S. E. Poulsen, S. Christensen and F. Joergensen, A synthetic study of geophysics-  
690 based modelling of groundwater flow in catchments with a buried valley, *Hydrogeology Journal*, 21,  
691 491-503, 2013.
- 692 Auken, E., A. V. Christiansen, J. H. Westergaard, C. Kirkegaard, N. Foged and A. Viezzoli, An  
693 integrated processing scheme for high-resolution airborne electromagnetic surveys, the SkyTEM system,  
694 *Exploration Geophysics*, 40(2), 184-192, 2009.
- 695 Babak, O. and C. V. Deutsch, An intrinsic model of coregionalization that solves variance inflation in  
696 collocated cokriging, *Computers & geosciences*, 35(3), 603-614, 2009.
- 697 Bowling, J. C., D. L. Harry, A. B. Rodriguez and C. M. Zheng, Integrated geophysical and geological  
698 investigation of a heterogeneous fluvial aquifer in Columbus Mississippi, *Journal of Applied*  
699 *Geophysics*, 62(1), 58-73, 2007.
- 700 Bredehoeft, J., The conceptualization model problem--surprise, *Hydrogeology Journal*, 13(1), 37-46,  
701 2005.
- 702 Caers, J., History matching under training-image-based geological model constraints, *Spe journal*, 8(3),  
703 218-226, 2003.
- 704 Caers, J. and T. Zhang, Multiple-point geostatistics: a quantitative vehicle for integrating geologic  
705 analogs into multiple reservoir models, Stanford University, Stanford Center for Reservoir Forecasting.  
706 California, USA, 2002.
- 707 Carle, S. F., T-PROGS: Transition Probability Geostatistical Software, University of California, Davis,  
708 1996.
- 709 Carle, S. F., Implementation schemes for avoiding artifact discontinuities in simulated annealing,  
710 *Mathematical Geology*, 29(2), 231-244, 1997.
- 711 Carle, S. F., Integration of Soft Data into Categorical Geostatistical Simulation. Not published  
712 manuscript, Water Resources Research, 2003.
- 713 Carle, S. F. and G. E. Fogg, Transition probability-based indicator geostatistics, *Mathematical Geology*,  
714 28(4), 453-476, 1996.
- 715 Carle, S. F. and G. E. Fogg, Modeling spatial variability with one and multidimensional continuous-lag  
716 Markov chains, *Mathematical Geology*, 29(7), 891-918, 1997.
- 717 Carle, S. F., G. S. Weissmann and G. E. Fogg, Conditional simulation of hydrofacies architecture: A  
718 transition probability approach, *SEPM Special Publication*, 1(1), 147-170, 1998.
- 719 Chugunova, T. L. and L. Y. Hu, Multiple-point simulations constrained by continuous auxiliary data,  
720 *Mathematical geosciences*, 40(2), 133-146, 2008.
- 721 dell'Arciprete, D., R. Bersezio, F. Felletti, M. Giudici, A. Comunian and P. Renard, Comparison of  
722 three geostatistical methods for hydrofacies simulation: a test on alluvial sediments, *Hydrogeology*  
723 *Journal*, 20(2), 299-311, 2012.



724 Deutsch, C. V. and P. W. Cockerham, Practical Considerations in the Application of Simulated  
725 Annealing to Stochastic Simulation, *Mathematical Geology*, 26(1), 67-82, 1994.

726 Deutsch, C. V. and A. Journel, *GSLIB: Geostatistical Software Library and Users Guide*, Oxford  
727 University Press, New York, 1992.

728 Deutsch, C. V. and X. H. Wen, Integrating large-scale soft data by simulated annealing and probability  
729 constraints, *Mathematical Geology*, 32(1), 49-67, 2000.

730 Emery, X. and J. Parra, Integration of crosswell seismic data for simulating porosity in a heterogeneous  
731 carbonate aquifer, *Journal of Applied Geophysics*, 98, 254-264, 2013.

732 Falivene, O., L. Cabrera, J. A. Munoz, P. Arbues, O. Fernandez and A. Saez, Statistical grid-based  
733 facies reconstruction and modelling for sedimentary bodies. Alluvial-palustrine and turbiditic examples,  
734 *Geologica Acta*, 5(3), 199-230, 2007.

735 Fleckenstein, J. H., R. G. Niswonger and G. E. Fogg, River-aquifer interactions, geologic heterogeneity,  
736 and low-flow management, *Ground Water*, 44(6), 837-852, 2006.

737 Gringarten, E. and C. V. Deutsch, Teacher's Aide Variogram Interpretation and Modeling, *Mathematical*  
738 *Geology*, 33(4), 507-534, 2001.

739 Gunnink, J. and B. Siemon, Combining airborne electromagnetics and drillings to construct a stochastic  
740 3D lithological model, 15th European Meeting of Environmental and Engineering Geophysics, Dublin,  
741 Ireland, 2009.

742 He, X., T. O. Sonnenborg, F. Jorgensen, A. S. Hoyer, R. R. Moller and K. H. Jensen, Analyzing the  
743 effects of geological and parameter uncertainty on prediction of groundwater head and travel time,  
744 *Hydrology and earth system sciences*, 17(8), 3245-3260, 2013a.

745 He, X., J. Koch, T. O. Sonnenborg, F. Jorgensen, C. Schamper and J. C. Refsgaard, Uncertainties in  
746 constructing stochastic geological models using transition probability geostatistics and transient AEM  
747 data., *Water Resources Research*, in revision, 2013b.

748 He, X., J. Koch, T. O. Sonnenborg, F. Jorgensen, C. Schamper and J. C. Refsgaard, Uncertainties in  
749 constructing stochastic geological models using transition probability geostatistics and transient AEM  
750 data., *Water Resources Research*, 2014.

751 Hojberg, A. L. and J. C. Refsgaard, Model uncertainty - parameter uncertainty versus conceptual  
752 models, *Water Science and Technology*, 52(6), 177-186, 2005.

753 Honarkhah, M. and J. Caers, Direct Pattern-Based Simulation of Non-stationary Geostatistical Models,  
754 *Mathematical geosciences*, 44(6), 651-672, 2012.

755 Hovadik, J. M. and D. K. Larue, Static characterizations of reservoirs: refining the concepts of  
756 connectivity and continuity, *Petroleum Geoscience*, 13(3), 195-211, 2007.

757 Hubbard, S. S. and Y. Rubin, Hydrogeological parameter estimation using geophysical data: a review of  
758 selected techniques, *Journal of contaminant hydrology*, 45(1-2), 3-34, 2000.

759 Jorgensen, F., H. Lykke-Andersen, P. B. E. Sandersen, E. Auken and E. Normark, Geophysical  
760 investigations of buried Quaternary valleys in Denmark: an integrated application of transient  
761 electromagnetic soundings, reflection seismic surveys and exploratory drillings, *Journal of Applied*  
762 *Geophysics*, 53(4), 215-228, 2003a.

763 Jorgensen, F., P. B. E. Sandersen and E. Auken, Imaging buried Quaternary valleys using the transient  
764 electromagnetic method, *Journal of Applied Geophysics*, 53(4), 199-213, 2003b.

765 Jorgensen, F., P. B. E. Sandersen, E. Auken, H. Lykke-Andersen and K. Sorensen, Contributions to the  
766 geological mapping of Mors, Denmark - A study based on a large-scale TEM survey, *Bulletin of the*  
767 *Geological Society of Denmark*, 52, 53-75, 2005.

768 Journel, A., Beyond covariance: the advent of multiple-point geostatistics., *Geostatistics Banff*.  
769 Springer, 1, 225-223, 2004.

770 Kemna, A., A. Binley and L. Slater, Crosshole IP imaging for engineering and environmental  
771 applications, *Geophysics*, 69(1), 97-107, 2004.

772 Krumbein, W. C. and M. F. Dacey, Markov Chains and Embedded Markov Chains in Geology,  
773 *Mathematical Geology*, 1(1), 79-96, 1969.

774 Lee, S. Y., S. F. Carle and G. E. Fogg, Geologic heterogeneity and a comparison of two geostatistical  
775 models: Sequential Gaussian and transition probability-based geostatistical simulation, *Advances in*  
776 *Water Resources*, 30(9), 1914-1932, 2007.

777 Linde, N., J. S. Chen, M. B. Kowalsky and S. Hubbard, Hydrogeophysical parameter estimation  
778 approaches for field scale characterization, SPRINGER, DORDRECHT, 2006.

779 Liu, Y. H., Using the Snesim program for multiple-point statistical simulation, *Computers &*  
780 *geosciences*, 32(10), 1544-1563, 2006.

781 Mariethoz, G., P. Renard, F. Cornaton and O. Jaquet, Truncated Plurigaussian Simulations to  
782 Characterize Aquifer Heterogeneity, *Ground Water*, 47(1), 13-24, 2009a.

783 Mariethoz, G., P. Renard and R. Froidevaux, Integrating collocated auxiliary parameters in geostatistical  
784 simulations using joint probability distributions and probability aggregation, *Water Resources Research*,  
785 45, W08421, 2009b.

786 McKenna, S. A. and E. P. Poeter, Field example of data fusion in site characterization, *Water Resources*  
787 *Research*, 31(12), 3229-3240, 1995.

788 Neuman, S. P., Maximum likelihood Bayesian averaging of uncertain model predictions, *Stochastic*  
789 *Environmental Research and Risk Assessment*, 17(5), 291-305, 2003.

790 Refsgaard, J. C., S. Christensen, T. O. Sonnenborg, D. Seifert, A. L. Hojberg and L. Trolborg, Review  
791 of strategies for handling geological uncertainty in groundwater flow and transport modeling, *Advances*  
792 *in Water Resources*, 36, 36-50, 2012.

793 Refsgaard, J. C., J. P. van der Sluijs, J. Brown and P. van der Keur, A framework for dealing with  
794 uncertainty due to model structure error, *Advances in Water Resources*, 29(11), 1586-1597, 2006.

795 Refsgaard, J. C., E. Auken, C. A. Bamberg, B. S. Christensen, T. Clausen, E. Dalgaard, F. Effersoe, V.  
796 Ernstsens, F. Gertz, A. L. Hansen, X. He, B. H. Jacobsen, K. H. Jensen, F. Joegensen, L. F. Joergensen, J.  
797 Koch, B. Nilsson, C. Petersen, G. De Schepper, C. Schamper, K. I. Soerensen, R. Therrien, C. Thirup  
798 and A. Viezzoli, Nitrate reduction in geologically heterogeneous catchments - a framework for  
799 assessing the scale of predictive capability of hydrological models., *Science of the Total Environment*, -  
800 (- 0), 2014.

801 Renard, P., Stochastic hydrogeology: What professionals really need?, *Ground Water*, 45(5), 531-541,  
802 2007.

803 Renard, P. and D. Allard, Connectivity metrics for subsurface flow and transport, *Advances in Water*  
804 *Resources*, 51, 168-196, 2013.

805 Ritzi, R. W., Behavior of indicator variograms and transition probabilities in relation to the variance in  
806 lengths of hydrofacies, *Water Resources Research*, 36(11), 3375-3381, 2000.

807 Rubin, Y., X. Y. Chen, H. Murakami and M. Hahn, A Bayesian approach for inverse modeling, data  
808 assimilation, and conditional simulation of spatial random fields, *Water Resources Research*, 46,  
809 W10523, 2010.

810 Schamper, C. and E. Auken, SkyTEM Survey Norsminde and Lillebaek. NiCA pproject 2011,  
811 HydroGeophysics Group. Aarhus University, 2011-06-16, 2012.

812 Seifert, D. and J. L. Jensen, Using sequential indicator simulation as a tool in reservoir description:  
813 Issues and uncertainties, *Mathematical Geology*, 31(5), 527-550, 1999.

814 Seifert, D., T. O. Sonnenborg, P. Scharling and K. Hinsby, Use of alternative conceptual models to  
815 assess the impact of a buried valley on groundwater vulnerability, *Hydrogeology Journal*, 16(4), 659-  
816 674, 2008.

817 Slater, L., Near surface electrical characterization of hydraulic conductivity: From petrophysical  
818 properties to aquifer geometries - A review, *Surveys in geophysics*, 28(2-3), 169-197, 2007.

819 Sorensen, K. I. and E. Auken, SkyTEM - a new high-resolution helicopter transient electromagnetic  
820 system, *Exploration Geophysics*, 35(3), 194-202, 2004.

821 Strebelle, S., Conditional simulation of complex geological structures using multiple-point statistics,  
822 *Mathematical Geology*, 34(1), 1-21, 2002.

823 Trolborg, L., J. C. Refsgaard, K. H. Jensen and P. Engesgaard, The importance of alternative  
824 conceptual models for simulation of concentrations in a multi-aquifer system, *Hydrogeology Journal*,  
825 15(5), 843-860, 2007.

826 Urish, D. W., Electrical Resistivity-Hydraulic Conductivity Relationships in Glacial Outwash Aquifers,  
827 *Water Resources Research*, 17(5), 1401-1408, 1981.

828 Weissmann, G. S., S. F. Carle and G. E. Fogg, Three dimensional hydrofacies modeling based on soil  
829 surveys and transition probability geostatistics, *Water Resources Research*, 35(6), 1761-1770, 1999.

830 Weissmann, G. S. and G. E. Fogg, Multi-scale alluvial fan heterogeneity modeled with transition  
831 probability geostatistics in a sequence stratigraphic framework, *Journal of Hydrology*, 226(1-2), 48-65,  
832 1999.

833 Ye, M. and R. Khaleel, A Markov chain model for characterizing medium heterogeneity and sediment  
834 layering structure, *Water Resources Research*, 44(9), 2008.

## Tables

Table 1. Split sample test showing how many of the high probable sand cells (resistivity > 60  $\Omega$ m) are simulated with corresponding sand probabilities (> 70%) or fully deterministic (probability = 1.0) among 25 realizations. Conditioned to onlyBH and onlySky20. The last column shows how many of the areas that are shown as sand in the boreholes are simulated with sand probabilities > 85%.

| <b>Conditioning<br/>Scenario</b> | <b>Prob. of sand &gt; 0.7<br/>AND<br/>resistivity &gt; 60 <math>\Omega</math>m</b> | <b>Prob. of sand = 1.0<br/>AND<br/>resistivity &gt; 60 <math>\Omega</math>m</b> | <b>Prob. of sand &gt; 0.85<br/>AND<br/>borehole = sand</b> |
|----------------------------------|------------------------------------------------------------------------------------|---------------------------------------------------------------------------------|------------------------------------------------------------|
| <b>onlyBH</b>                    | 20.1 %                                                                             | 1.34 %                                                                          | 74.3 %                                                     |
| <b>onlySky20</b>                 | 99.0 %                                                                             | 59.1%                                                                           | 44.0 %                                                     |

Table 2. Proportion of high probable sand cells (resistivity > 60  $\Omega$ m) that are simulated with corresponding sand probabilities (> 70%) or fully deterministic (probability = 1.0) for six conditioning datasets based on 25 realizations.

| Conditioning Dataset                         | Prob. of sand > 0.7<br>AND<br>resistivity > 60 $\Omega$ m | Prob. of sand = 1.0<br>AND<br>resistivity > 60 $\Omega$ m |
|----------------------------------------------|-----------------------------------------------------------|-----------------------------------------------------------|
| <b>BH-Sky20static</b>                        | 97.9 %                                                    | 63.8 %                                                    |
| <b>BH-Sky100static /<br/>BH-Sky100moving</b> | 84.1 % / 87,3                                             | 10.4 % / 10.1 %                                           |
| <b>BH-Sky200static /<br/>BH-Sky200moving</b> | 75.8 % / 71.0 %                                           | 5.4% / 3.6 %                                              |
| <b>BH-Sky500static</b>                       | 32.7 %                                                    | 1.5 %                                                     |

Table 3. Simulated and defined sand proportions for the total domain and two sub-domains based on two simulations with different soft conditioning datasets (BH-Sky20static and BH-Sky200moving), based on 25 realizations.

| Mean sand proportion (%) based on 25 realizations | BH-Sky20static |       |       |
|---------------------------------------------------|----------------|-------|-------|
|                                                   | Total          | South | North |
| Defined                                           | 23             | 30    | 13    |
| Simulated                                         | 25.0           | 30.7  | 13.8  |
| Deviation                                         | +2.0           | +0.7  | +1.8  |
| BH-Sky200moving                                   |                |       |       |
| Defined                                           | 23             | 30    | 13    |
| Simulated                                         | 29.3           | 33.7  | 21.5  |
| Deviation                                         | +6.3           | +3.7  | +8.5  |

Table 4. The five performance criteria and categorized SkyTEM data as benchmark that are applied to the two simulations with different soft conditioning datasets: Cell by cell soft conditioning and 200m moving sampling soft conditioning; both including borehole data. The first three criteria are expressed as deviation to the benchmark.

| Performance Criteria                        | Categorized SkyTEM | BH-Sky20static                            | BH-Sky200moving                                 |
|---------------------------------------------|--------------------|-------------------------------------------|-------------------------------------------------|
| 1. Sand proportion                          | 23%                | +2%                                       | +6.3%                                           |
| 2. Mean length (X/Y)                        | 500m               | -21% / -20%                               | -37% / -37%                                     |
| 3. Geobody Connectivity ( $\theta/\Gamma$ ) | 98.7% / 99.3%      | -2.1% / -1.1%                             | -2.8% / -1.4%                                   |
| 4. Facies probability distribution          | n.a.               | Poor (approx. 70% cells with zero change) | Satisfying (approx. 15% cells with zero change) |
| 5. Facies probability-resistivity bias      | n.a.               | 0.20                                      | 0.06                                            |

## Figure Captions

Figure 1. The study site in eastern Jutland, Dk. The Norsminde catchment with the delineated glacial structure in the western part of the catchment. Additionally the river network and the topography.

Figure 2: Side-by-side comparison of borehole lithological data and SkyTEM vertical sounding data at borehole number 99.625 (He. et. al, 2014).

Figure 3. The median resistivity values from the SkyTEM data for the 4- and 16- subarea grid. Dark colors indicate a high median (max: 43.2  $\Omega\text{m}$  and 45.0  $\Omega\text{m}$  for the 4- and 16- subarea grid, respectively), light colors a low median (min: 32.0  $\Omega\text{m}$  and 29.5  $\Omega\text{m}$  for the 4- and 16- subarea grid, respectively) and white colors the absence of data. Additionally the location of the boreholes, the river network and the delineated glacial structure. The extent is 9km in X- and 12km in Y-direction.

Figure 4. The bias corrected histogram curve: The calibrated cut off value (46  $\Omega\text{m}$ ) is added to the histogram and the fitted curve is forced to honor it He et al. (2013).

Figure 5. The computed transition probabilities in vertical and horizontal direction and the fitted MCM: Vertical 5m, horizontal 500m mean length of a sand lens and 23% sand proportion. Additionally the fitted MCM for the north- and south-sub-domain are plotted for the vertical and horizontal sand-sand transitions: 2m, 400m, 13% and 5m, 600m, 30%, respectively.

Figure 6. Upper panel: Two individual realizations for two different conditioning scenarios: onlyBH (a) and onlySky20 data (b). Lower panel: Probability maps for the two scenarios c) and e) showing the probability of sand in each cell based on 25 realizations. The derived sand probability which is used for conditioning the simulation is shown in (d). All maps show data at an elevation of 49m.

Figure 7. The simulated versus the conditioned sand probability over the vertical extent at one borehole (98.918), located in the south western part of the glacial structure. The results originate from the two different soft conditioning scenarios: onlyBH and onlySky20 (based on 25 realizations each).

Figure 8. a): 100 m (small dots) and 500 m (big dots) sampling grids for thinning out the conditioning dataset; b-e): probability of sand at an elevation of 49 m for SkyTEM dataset (b), and for static 20m, 200m and 500m conditioning (c-e) Red colors represent high sand probability and blue colors low sand probability (based on 25 realizations).

Figure 9. The simulated transition probabilities for the south-, north-, and total-domain are compared with the SkyTEM data and the fitted MCM. The results for two soft conditioning dataset are shown: BH-Sky20static and BH-Sky200moving. The simulated TP and the MCM at lag 100m are compared to quantify the underestimation of a sand lens. The TP values are mean values based on 10 realizations. The defined length of a sand lens ( $X$ ) and the mean simulated length for the BH-Sky20static ( $Y$ ) and BH-Sky200moving scenario ( $Z$ ) are given in each graph. ( $X_m - Y_m / Z_m$ ).

Figure 10. The simulated facies probability distributions based on sets of realizations conditioned to differently sampled soft datasets (based on 25 realizations): (a) static sampling at different sampling distances and (b) stationary and moving sampling at different sampling distances. Also showing the sand probability distribution of the original soft dataset which is desired to be reproduced.

Figure 11. The simulated facies probability – resistivity bias based on sets of realizations conditioned to differently sampled soft datasets (based on 25 realizations): (a) static sampling at different sampling distances and (b) stationary and moving sampling at different sampling distances. The simulated sand probability is paired with the original resistivity value, grouped into 5  $\Omega\text{m}$  bins and then plotted as median for each bin. Also showing the observed data and the fitted curve from the histogram which is desired to be reproduced.



## Figures

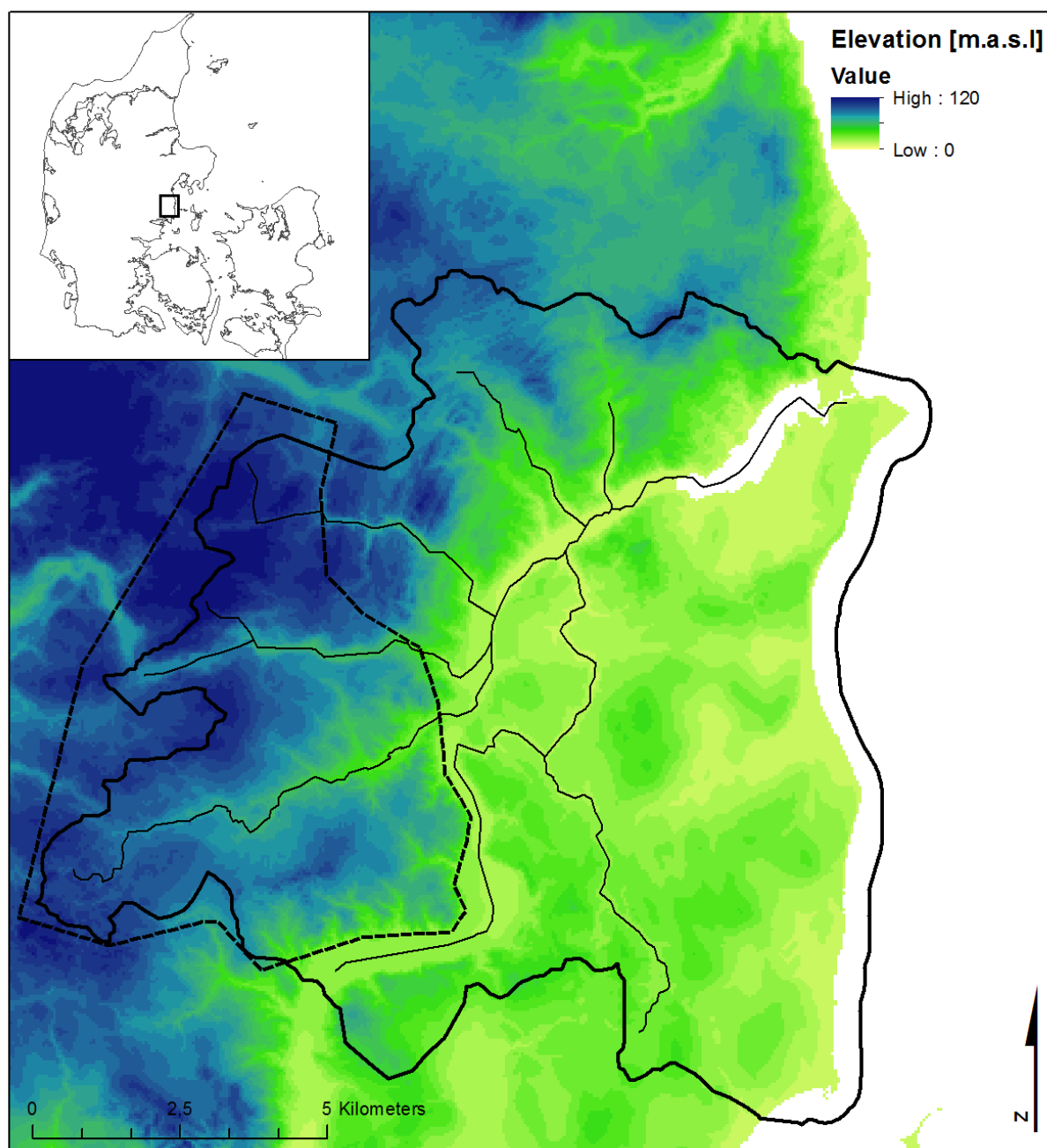
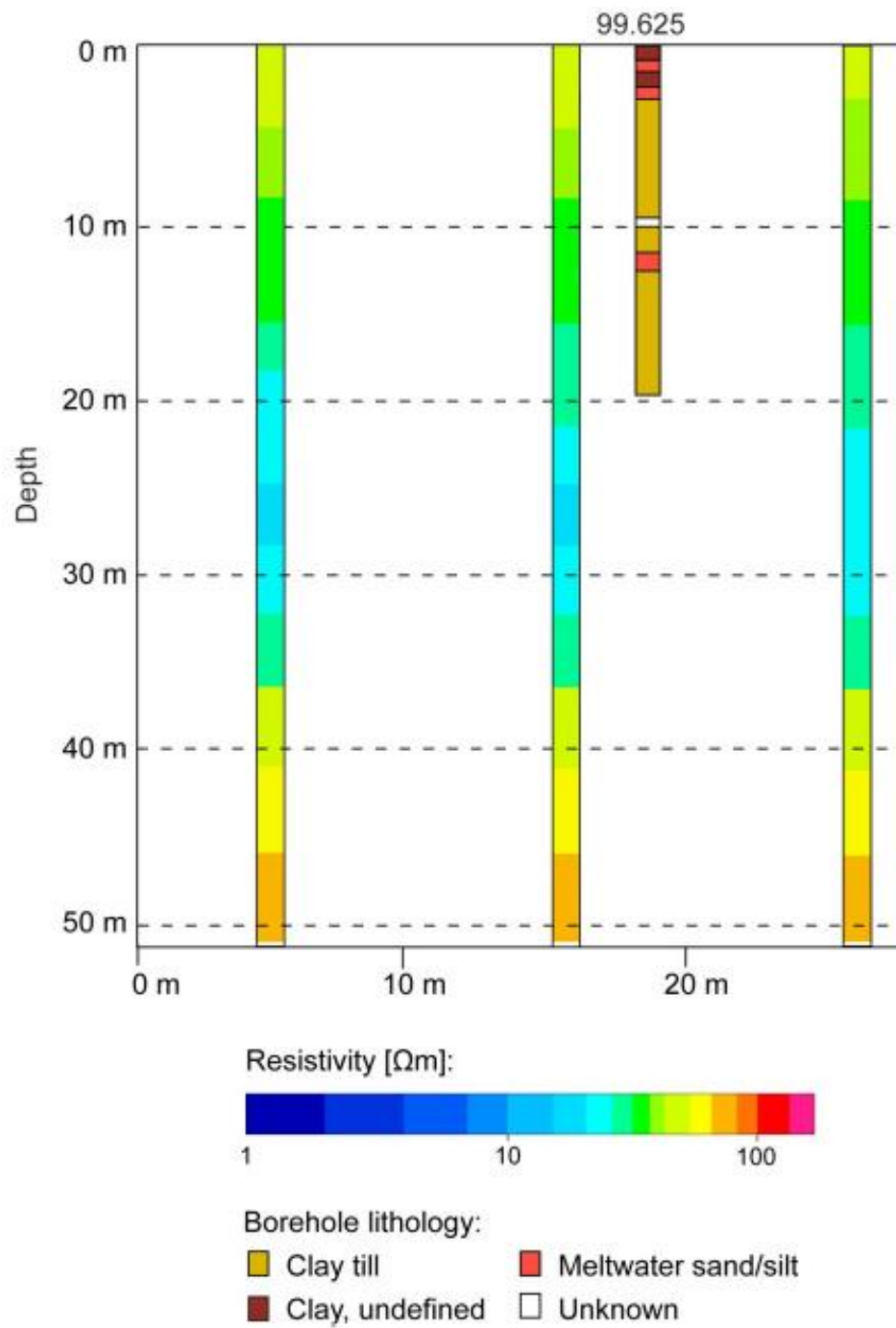


Figure 1. The study site in eastern Jutland, Dk. The Norsminde catchment with the delineated glacial structure in the western part of the catchment. Additionally the river network and the topography.



Figur 2 Side-by-side comparison of borehole lithological data and SkyTEM vertical sounding data at borehole number 99.625 (He. et. al, 2014).

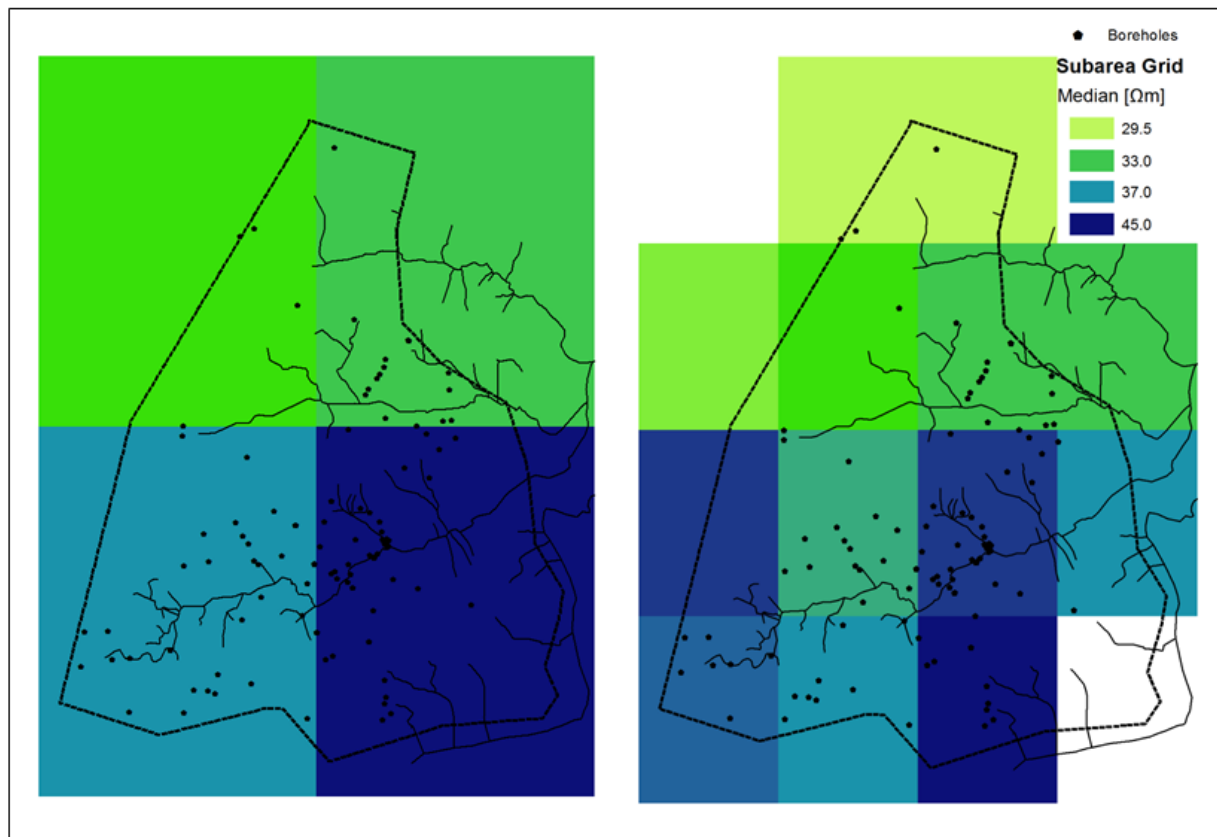


Figure 3. The median resistivity values from the SkyTEM data for the 4- and 16- subarea grid. Dark colors indicate a high median (max: 43.2  $\Omega\text{m}$  and 45.0  $\Omega\text{m}$  for the 4- and 16- subarea grid, respectively), light colors a low median (min: 32.0  $\Omega\text{m}$  and 29.5  $\Omega\text{m}$  for the 4- and 16- subarea grid, respectively) and white colors the absence of data. Additionally the location of the boreholes, the river network and the delineated glacial structure. The extent is 9km in X- and 12km in Y-direction.

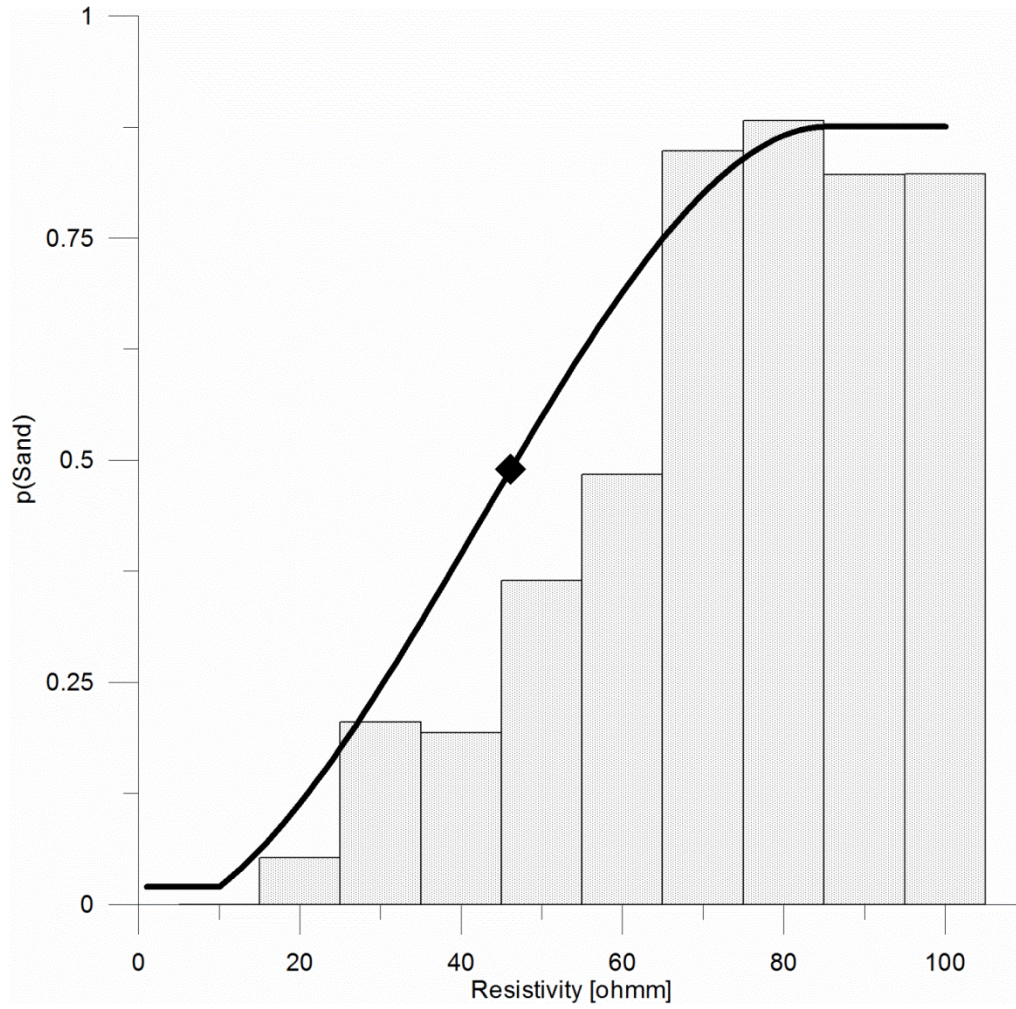


Figure 4. The bias corrected histogram curve: The calibrated cut off value (46  $\Omega\text{m}$ ) is added to the histogram and the fitted curve is forced to honor it He et al. (2014).

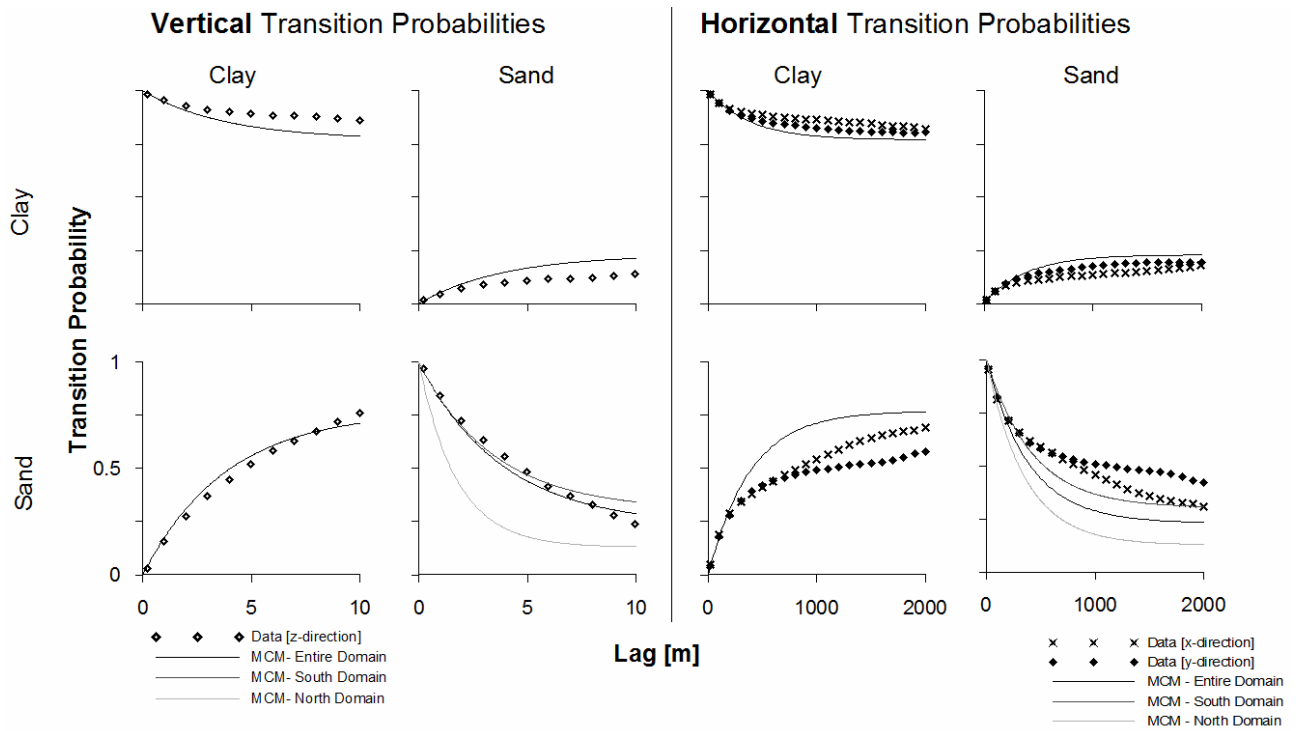


Figure 5. The computed transition probabilities in vertical and horizontal direction and the fitted MCM: Vertical 5m, horizontal 500m mean length of a sand lens and 23% sand proportion. Additionally the fitted MCM for the north- and south-sub-domain are plotted for the vertical and horizontal sand-sand transitions: 2m, 400m, 13% and 5m, 600m, 30%, respectively.

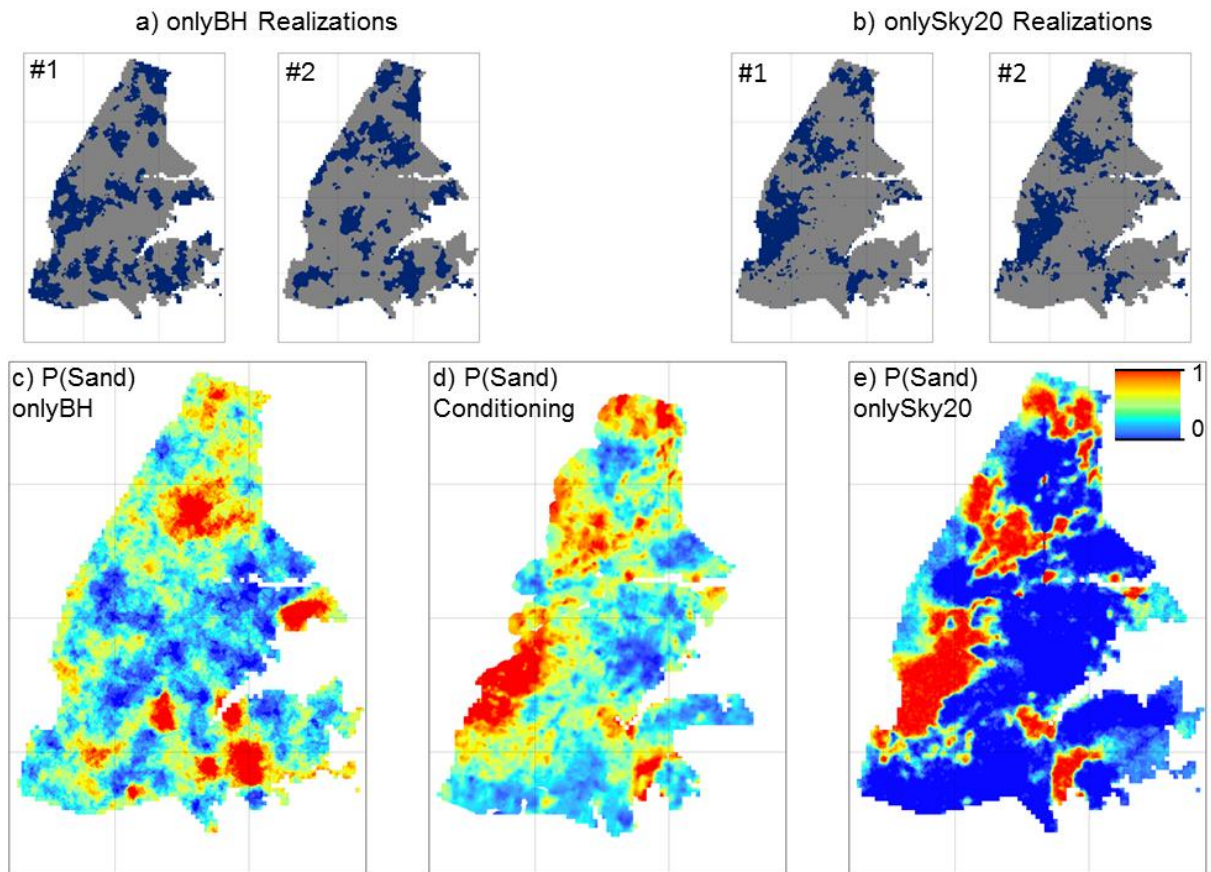


Figure 6. Upper panel: Two individual realizations for two different conditioning scenarios: *onlyBH* (a) and *onlySky20* data (b). Lower panel: Probability maps for the two scenarios c) and e) showing the probability of sand in each cell based on 25 realizations. The derived sand probability which is used for conditioning the simulation is shown in (d). All maps show data at an elevation of 49m.



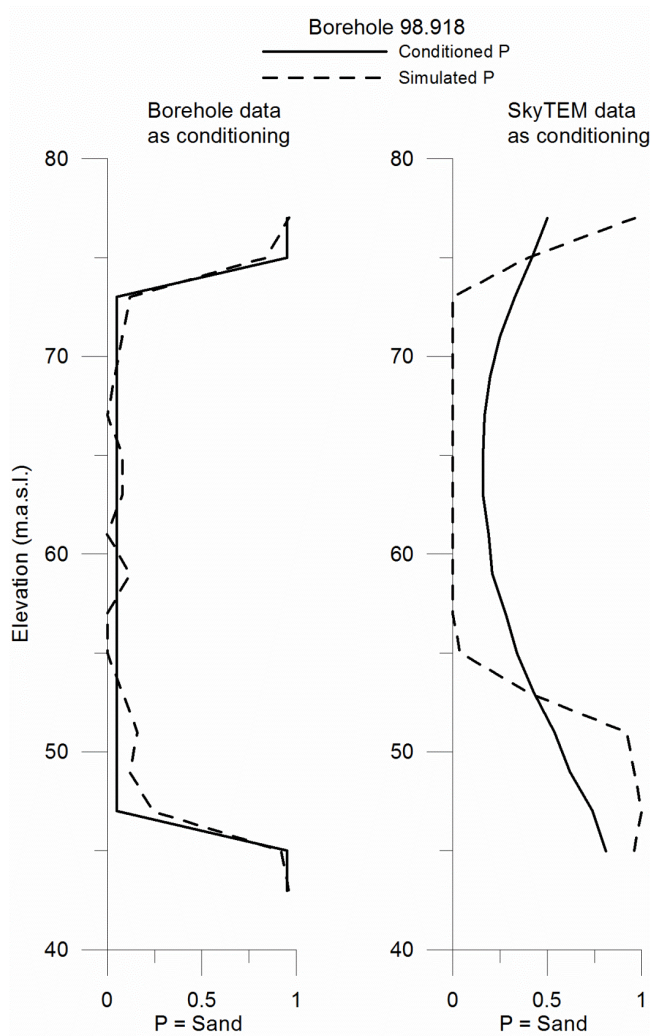


Figure 7. The simulated versus the conditioned sand probability over the vertical extent at one borehole (98.918), located in the south western part of the glacial structure. The results originate from the two different soft conditioning scenarios: *onlyBH* and *onlySky20* (based on 25 realizations each).

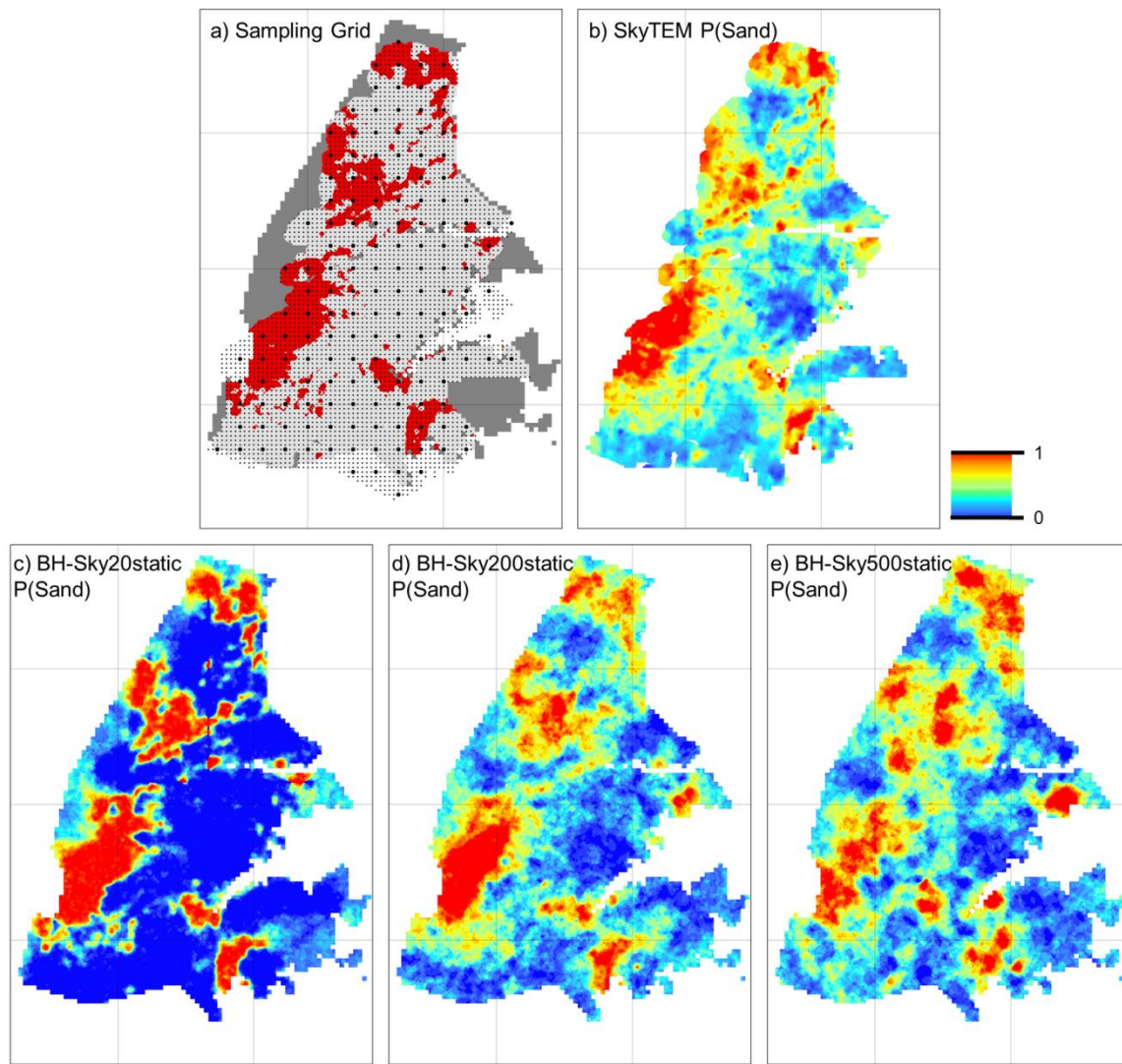


Figure 8. a): 100 m (small dots) and 500 m (big dots) sampling grids for thinning out the conditioning dataset; b-e): probability of sand at an elevation of 49 m for SkyTEM dataset (b), and for static 20m, 200m and 500m conditioning (c-e) Red colors represent high sand probability and blue colors low sand probability (based on 25 realizations).



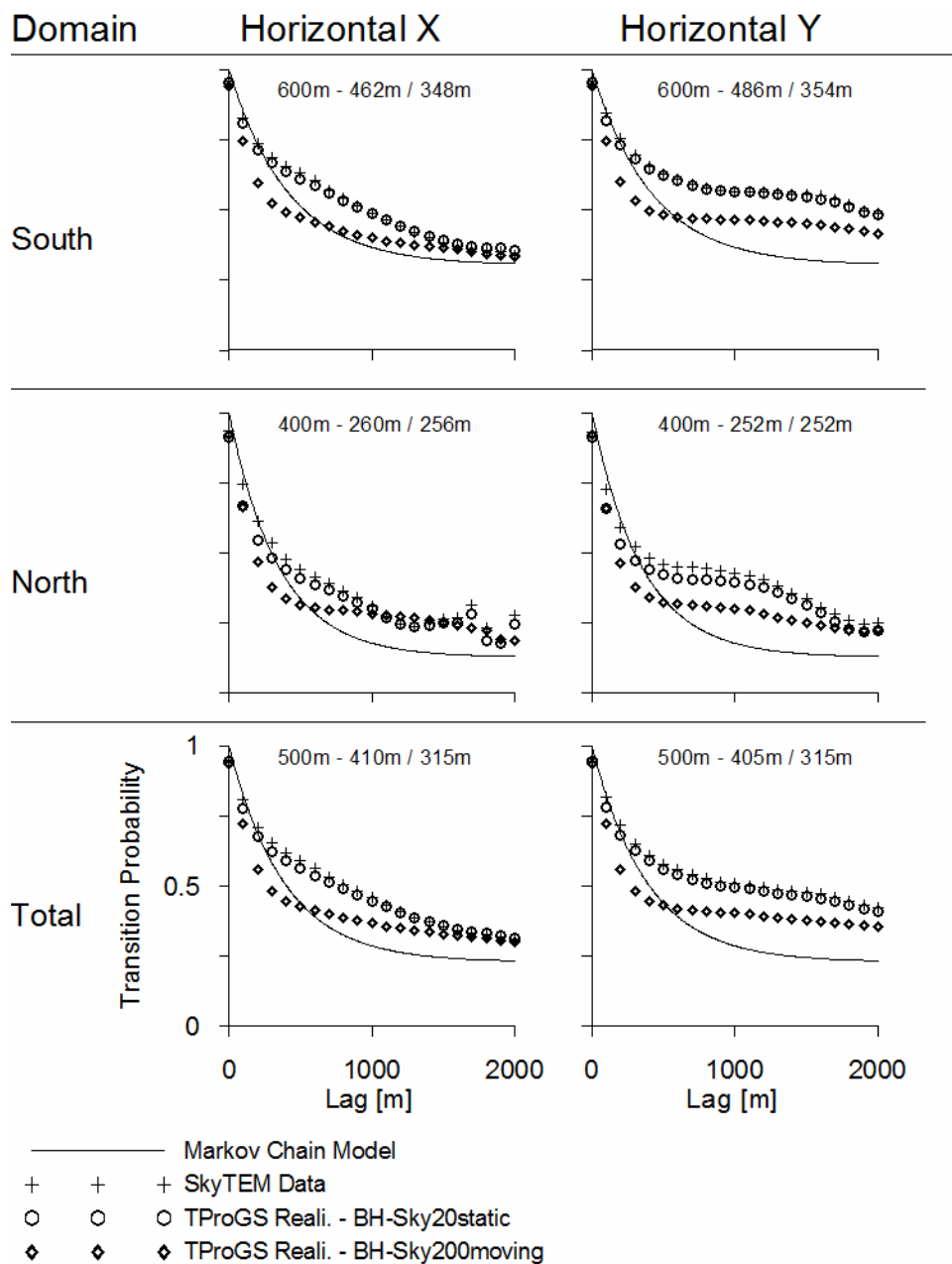


Figure 9. The simulated transition probabilities for the south-, north-, and total-domain are compared with the SkyTEM data and the fitted MCM. The results for two soft conditioning dataset are shown: *BH-Sky20static* and *BH-Sky200moving*. The simulated TP and the MCM at lag 100m are compared to quantify the underestimation of a sand lens. The TP values are mean values based on 10 realizations. The defined length of a sand lens (X) and the mean simulated length for the *BH-Sky20static* (Y) and *BH-Sky200moving* scenario (Z) are given in each graph. ( $X_m - Y_m / Z_m$ ).

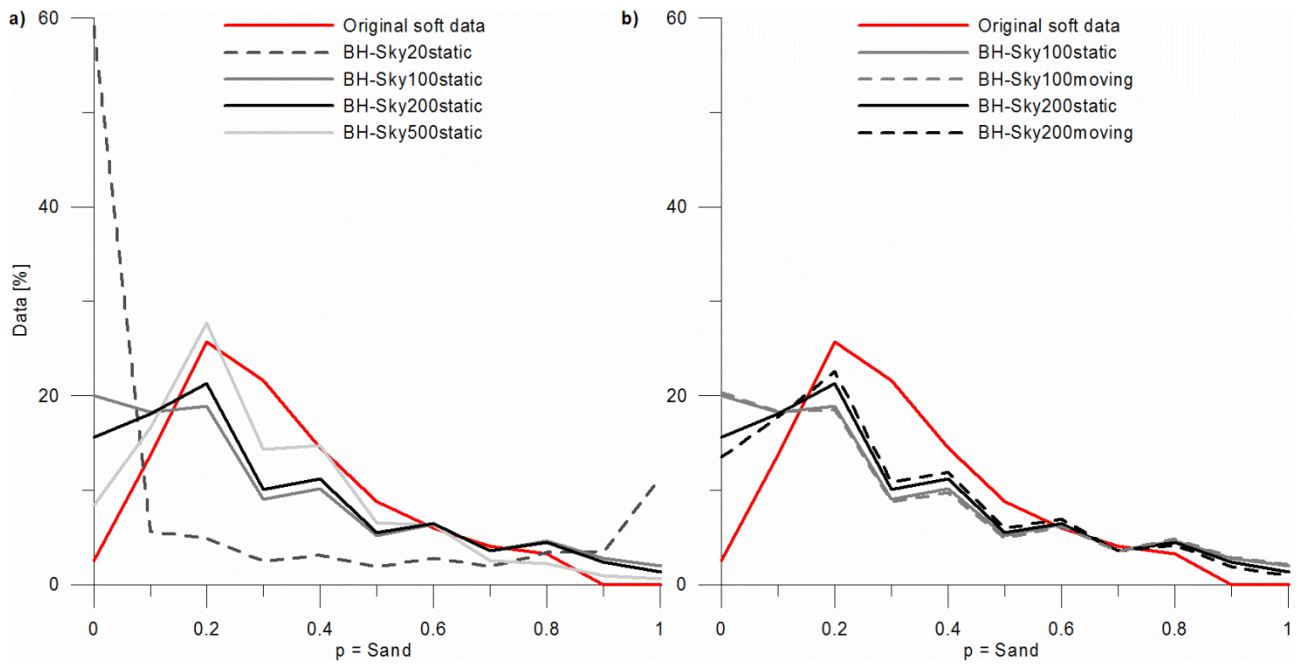


Figure 10. The simulated facies probability distributions based on sets of realizations conditioned to differently sampled soft datasets (based on 25 realizations): (a) static sampling at different sampling distances and (b) stationary and moving sampling at different sampling distances. Also showing the sand probability distribution of the original soft dataset which is desired to be reproduced.

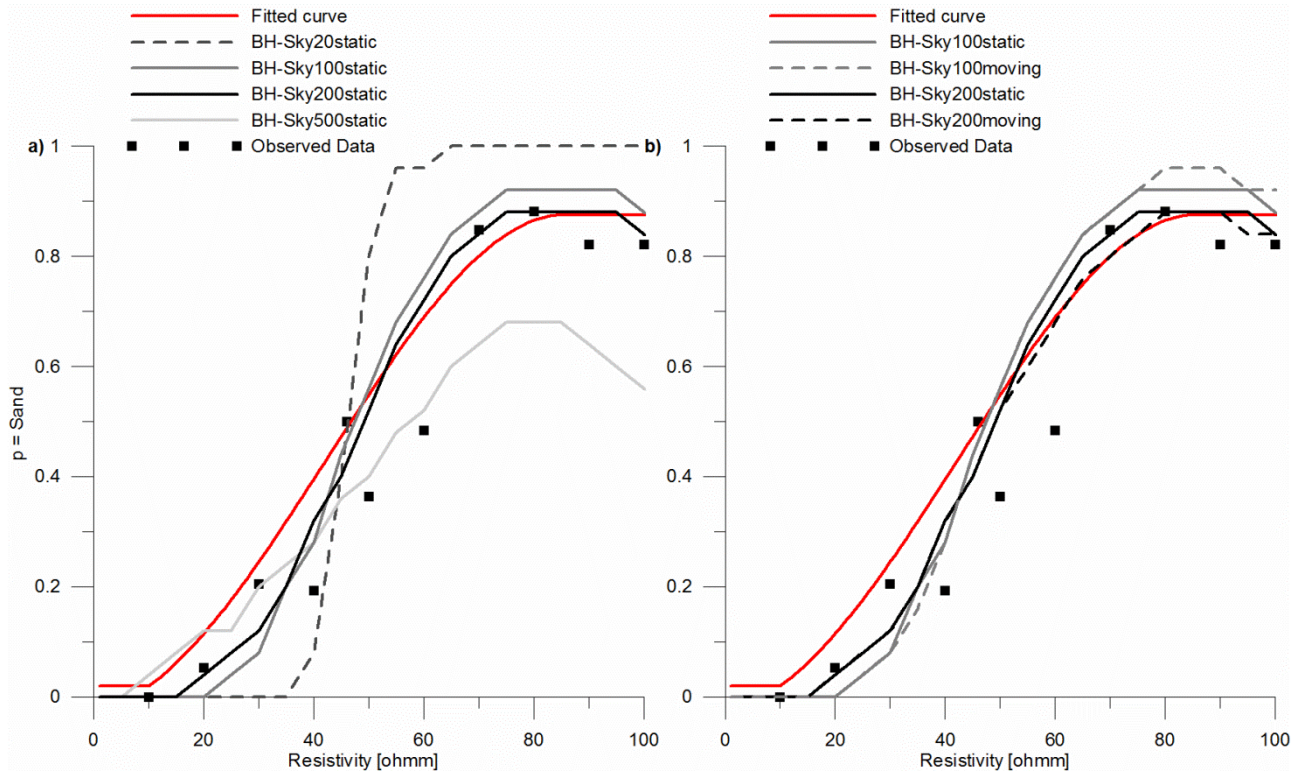


Figure 11. The simulated facies probability – resistivity bias based on sets of realizations conditioned to differently sampled soft datasets (based on 25 realizations): (a) static sampling at different sampling distances and (b) stationary and moving sampling at different sampling distances. The simulated sand probability is paired with the original resistivity value, grouped into 5  $\Omega\text{m}$  bins and then plotted as median for each bin. Also showing the observed data and the fitted curve from the histogram which is desired to be reproduced.